Nonlinear Tropical Air–Sea Interaction in the Fast-Wave Limit

ZHENG HAO, J. DAVID NEELIN, AND FEI-FEI JIN

Department of Atmospheric Sciences, University of California at Los Angeles, Los Angeles, California

(Manuscript received 5 June 1992, in final form 15 December 1992)

ABSTRACT

The fast-wave limit is an approximation useful for understanding many aspects of tropical air–sea interaction. It is obtained when the time scale of dynamical adjustment of the ocean by equatorial waves occurs fast compared to the time scale on which the system is evolving through coupled processes. The linear and nonlinear behavior of a simple coupled model is examined for the Pacific basin. It consists of an SST equation for an equatorial band, shallow-water ocean dynamics in the fast-wave limit governing the thermocline, and an embedded surface layer for equatorial Ekman pumping; it may be characterized as a simple fast-wave limit version of the Neelin model, which is in turn a stripped-down version of the Zebiak and Cane model. It offers a converse approximation to simple models that retain wave dynamics while eliminating SST time scales.

This simple model produces a rich variety of flow regimes. The first bifurcation can give westward-propagating, stationary, or eastward-propagating variability according to the relative strength of the surface-layer and thermocline processes and the atmospheric damping length. These parameter dependences can be largely explained by reference to the simpler zonally periodic case, but the finite basin and zonally varying basic state introduce east basin trapping. These weakly nonlinear regimes offer a simple analog of oscillations in a number of other models. Some of the oscillations show thermocline evolution that could be easily mistaken for wave-dependent behavior in other models. Over a substantial region of parameter space, two SST modes—one stationary and one westward-propagating—have comparable growth rate in the linear problem. This introduces mode interaction in the nonlinear problem. Relaxation oscillations at strong nonlinearity prove to be a very robust feature of the model, showing strong parallels to behavior noted in a hybrid coupled general circulation model.

1. Introduction

The El Niño–Southern Oscillation (ENSO) phenomenon is among the dominant sources of interannual climate variability (e.g., Bjerknes 1969; Rasmusson and Carpenter 1982; Graham et al. 1987; Deser and Wallace 1990; Rasmusson et al. 1990; Barnett 1991; Ghil and Vautard 1991). It is now generally understood that ENSO arises through interaction between the tropical atmosphere and the tropical Pacific Ocean. A number of models of varying levels of complexity have captured interannual variability resembling ENSO. These include full coupled ocean–atmosphere general circulation models (GCMs) (e.g., Meehl 1990; Philander et al. 1992; Lau et al. 1992; Neelin et al. 1992a; Nagai et al. 1992; Latif et al. 1993), hybrid coupled GCMs consisting of an ocean GCM coupled to a simpler atmospheric model (Neelin 1989a, 1990a; Latif and Villwock 1990), intermediate models (e.g., Zebiak and Cane 1987; Battisti 1988; Anderson and McCreary 1985), and a variety of simpler models. The latter include linear instability studies used for understanding how large-scale coupled air–sea interaction gives rise to the interannual oscillations (e.g., Philander et al. 1984; Hirst 1986, 1988; Wakata and Sarachik 1991).

Because subsurface memory associated with dynamical adjustment processes appears to play a significant role in setting the time scale of oscillation in some models and apparently in the observed ENSO, considerable attention has been given to a simple differential-delay equation postulated by Suarez and Schopf (1988) to explain the results of the Schopf and Suarez (1988) model. A modified form of this "delayed-oscillator" model was shown by Battisti and Hirst (1989) to give a reasonable fit to the behavior of the Battisti (1988) version of the Zebiak and Cane (1987) model. In this model, local air–sea interaction in the eastern part of the basin is assumed to produce a pure growth tendency, while a delay representing the transit time of Rossby wave propagation to the western boundary and Kelvin wave propagation back to the coupling region is essential for oscillation. More realistic formulations of simple models in which equatorial wave time scales are crucial to the dynamics are given by Cane et al. (1990) and Schopf and Suarez (1990). A debate regarding the relevance of observations of off-equatorial Rossby waves to this mechanism may be found in Graham and White (1988) versus Battisti (1989).

Interannual oscillations, however, are also possible in which the time scale of wave dynamics does not play

Corresponding author address: Dr. J. David Neelin, Department of Atmospheric Sciences, University of California, Los Angeles, 405 Hilgard Ave, Los Angeles, CA 90024-1565.

© 1993 American Meteorological Society

a crucial role. Neelin (1991; N91 hereafter) introduced the "fast-wave limit" as a useful approximation to such oscillations. In this limit, dynamical adjustment by equatorial waves occurs on time scales much faster than the time scale of SST evolution by coupled processes. Wave dynamics is important in setting up the ocean state at any given time, but the time scale is not important to the coupled dynamics. The slow modes in this limit are referred to as "SST modes" since they are associated with the time derivative of the SST equation, although their form and time scale is strongly determined by coupled processes. Neelin (1991) provides simple analytic solutions for SST modes in the fast-wave limit for the periodic-basin case and shows by distorted physics experiments that the fast-wave limit provides a useful approximation to the oscillations in certain flow regimes in a hybrid coupled GCM.

Jin and Neelin (1993a,b) and Neelin and Jin (1993) (collectively referred to as JN hereafter) show that the various modes are all fundamentally related, although they exhibit different behavior in different parts of parameter space. The linear models of Cane et al. (1990) and Schopf and Suarez (1990) and the nonlinear model of Münnich et al. (1991) are formulated in a special case of the "fast-SST limit," the converse to the fast-wave limit, in which the time scale of SST is assumed to adjust quickly compared to the time scale of equatorial wave adjustment. By examining the eigenmodes of the system, linearized about climatology, JN show that most important modes in the fast-wave limit and in the fast-SST limit are continuously connected and that these limits offer alternate approximations to the same eigensurface. In the most realistic part of parameter space, both wave time scales and SST time scales are important to the mixed SST/ocean dynamics modes. The very different regimes of behavior for these modes within a small region of parameter space help to explain the variety of results obtained for interannual phenomena in coupled GCMs (Neelin et al. 1992a).

Our purpose here is to examine the nonlinear behavior of SST modes in the fast-wave limit in a finite basin. A linear analysis of the modes leading to the primary bifurcations is included as a prelude to the nonlinear results. The model includes an SST equation similar to that used in intermediate models, and because this includes the most important nonlinearities, considerable insight into the flow regimes can be gained from this case. The only qualitative difference to be expected is that some of the bifurcations that appear in this model as stationary bifurcations would have oscillatory counterparts in a model with finite wave time scales. A surface of codimension-two bifurcations separates these regimes, as discussed in JN. Any stationary state of the system at finite wave time scales, on the other hand, has an identical solution in the fast-wave limit. We emphasize that the model is intended to offer a converse approximation to the assumptions of the fast-SST limit models such as Cane et al. (1990) and that the fundamental questions of interest are 1) what nonlinear coupled behavior can be found in a coupled model that does not depend on wave time scales, and 2) how this can inform our analysis of more complex coupled models.

We limit our examination to the use of forward time integration and the eigenvalue problem for the system linearized about a climatological stationary state. The time integration provides an indication of the transient behavior as well as the attractors of the system in a manner comparable to that available in more complex models. The primary bifurcations are all easily identifiable from this and the linear analysis. It also provides a good indication of the types of higher bifurcations and strongly nonlinear flow regimes that would be encountered in a more thorough exploration. Because the climatological stationary state is constructed by flux correction in a manner similar to hybrid and intermediate coupled models, bifurcations involving large-amplitude anomalies are not necessarily realistic but they can provide insight into similar regimes in the more complex models. We outline parallels between this and more complex models in the spatial and temporal evolution of the flow field in the various regimes. The complexity of the phenomena that arise even without wave time scales proves to be remarkable.

After describing the model in section 2, we present the linear analysis in section 3 and nonlinear results in section 4. In both cases, the dependence of the system on coupling strength, atmospheric damping length, and the relative strength of surface-layer and thermocline feedbacks is examined. Section 5 provides summary and discussion.

2. The model

The strongest SST response to upwelling, zonal advection, and thermocline depth anomalies is confined to a fairly narrow band along the equator for the phenomena being considered. Although observed SST anomalies may have somewhat different meridional scales at different longitudes, for purposes of understanding, the SST anomaly can be taken to have fixed meridional structure. The N91 model exploits this by treating the SST equation for an equatorial band, with fixed meridional dependence of the forcing felt by the atmospheric component. The resulting model is essentially a stripped-down version of the Zebiak and Cane (1987) intermediate model, exhibiting most of the most crucial dynamics, but is simple enough to solve analytically in some cases. Although the model is three-dimensional (albeit with limited vertical degrees of freedom), in the fast-wave limit it reduces to a partial differential equation in longitude and time only. The version used here is closely related to a fast-wave limit version of the model presented in Neelin and Jin (1993).

a. Atmospheric component

The atmospheric component is a simplified version of the Gill (1980) model. Since the atmospheric adjustment time is fast compared with the time scales of the ocean and the ENSO cycle, the atmosphere is assumed to be instantaneously in equilibrium with the oceanic evolution. The atmospheric model equations on the equatorial β plane, under standard nondimensionalization, are just

$$\epsilon_a^* u_a - y_a v_a + \partial_x \phi = 0, \tag{2.1a}$$

$$y_a u_a + \partial_{y_a} \phi = 0, \tag{2.1b}$$

$$\epsilon_a^* \phi + \partial_x u_a + \partial_{y_a} v_a = -Q, \tag{2.1c}$$

where ϵ_a^* is a nondimensionalized Rayleigh friction due to boundary-layer turbulence; u_a, v_a and ϕ are boundary-layer winds and geopotential perturbations, respectively; and Q is a forcing term that is closely related to latent heating and is parameterized to be proportional to the SST perturbation, an approximation that may be justified in terms of several physical mechanisms (Lindzen and Nigam 1987; Neelin and Held 1987; Neelin 1989b).

As the atmosphere and oceans have different meridional length scales, the SST perturbation is projected onto Hermite functions, $\psi_n(y_a)$, where y_a is meridional distance normalized to the atmospheric radius of deformation:

$$Q = T'(x) \sum_{n=0}^{\infty} S_n(x)\psi_n(y_a).$$

Wind stress on the ocean surface is by definition proportional to the atmospheric boundary-layer wind. The zonal wind stress anomaly along the equator can thus be written as

$$\tau' = \mu \frac{1}{2} A \epsilon_a \Bigg\{ -S_0 e^{-\epsilon_a x} \int_{x_W}^{x} T'(s) e^{\epsilon_a s} ds - \sum_{n=2}^{\infty} (-1)^{n/2} \frac{n!}{(n/2)!} \frac{2n-1}{(n-1)} \left[(n-1) S_n + \frac{1}{2} S_{n-2} \right] \times e^{(2n-1)\epsilon_a x} \int_{x}^{x_E} T'(s) e^{-(2n-1)\epsilon_a s} ds \Bigg\}, \tag{2.2}$$

where the sum is over even values of n and where ϵ_a is the Rayleigh friction redimensionalized as an inverse damping length scale. The amplitude factor A measures the strength of the wind stress feedback per unit SST anomaly for standard values of the atmospheric model, while the relative coupling coefficient μ is a convenient parameter for changing the strength of the coupling. It is convenient to scale wind stress by $(\rho H)^{-1}$, the mass per unit area of the ocean above the thermocline, so $A = A^*/(\rho H)$, with A^* in Pa K^{-1}, and τ' thus denotes the acceleration due to zonal wind stress on the ocean. The value of A^* used here is on the high side (compared for instance to JN), resulting in bifurcations at correspondingly lower μ.

Two alternate cases have been used for the meridional structure of the atmospheric forcing. The first assumes that the SST perturbation projects primarily onto S_0, that is, that the SST structure can be approximated by a Gaussian with a half-width of the atmospheric radius of deformation, typically estimated in the range 5°–10° latitude. Since this is somewhat larger than typical SST or heating anomalies, the effects of using a delta-function y dependence (i.e., very narrow Q) were tested as an alternate approximation. For this case, $S_n = \pi^{-1/2}(-1)^{n/2}2^{-n}\,[1/(n/2)!]$ and the series must be carried to fairly large truncation. The wind stress near the equator is rather similar to the S_0 case, however, and numerical runs with both formulas show similar evolutions of SST. The bifurcations are slightly shifted between the two cases, but the qualitative behavior is extremely similar. Therefore, the runs presented here are all with the simpler case, for which

$$\tau' = \mu \epsilon_a A \left[\frac{3}{2} e^{3\epsilon_a x} \int_{x}^{x_E} T'(s) e^{-3\epsilon_a s} ds - \frac{1}{2} e^{-\epsilon_a x} \int_{x_W}^{x} T'(s) e^{\epsilon_a s} ds \right]. \tag{2.3}$$

b. Ocean component

1) OCEAN COMPONENT EQUATIONS

The ocean component is based on a modified shallow-water model with a fixed-depth mixed layer and a lower undercurrent layer (Cane 1979), and is closely related to the model employed in N91 and JN except that only the fast-wave limit is considered.

The SST equation governs the thermodynamics of a box whose depth is that of the upper mixed-layer, H_1, and whose width, L_y, is characteristic of the width of upwelling. Since temperatures outside the box are fixed or parameterized, an upstream advection scheme is employed for vertical and meridional advection to ensure suitable behavior. For total SST, this gives

$$\partial_t T + \mathscr{H}(w) \frac{w}{H_{1\,1/2}} (T - T_{sub}) - \mathscr{H}(-v_N) \frac{2v_N}{L_y} \times (T - T_N) + \epsilon_T (T - T_0) = 0, \tag{2.4}$$

where T is the temperature of the equatorial surface box and $\mathscr{H}(w) = \frac{1}{2}(\tanh(w/\Delta w) + 1)$ is a continuous approximation to the Heaviside function used to switch between upwelling and downwelling cases in the upstream differencing scheme. As $\Delta w \to 0$, $\mathscr{H}$ approaches the Heaviside function ($\Delta w = 1$ cm day^{-1} is used, two orders of magnitude less than typical $\bar{w}$ values). The use of analytic functions ensures nice properties for the phase-space flow. The Newtonian cooling term, with

inverse damping time, ϵ_T, represents all one-dimensional vertical processes, which include mixing, sea surface sensible and latent heat fluxes, and longwave and shortwave radiation. Here T_0 is the equatorial SST value at the state of radiative–convective mixing equilibrium in absence of large-scale horizontal dynamics in the upper ocean or atmosphere; T_N is the fixed off-equatorial SST, which could be specified as a function of longitude but is here treated as constant. North–south asymmetries in off-equatorial SST are not treated here. Zonal advection of SST is neglected in (2.4); in the linear case, it acts similarly to upwelling perturbations and tends to be smaller (in the fast-wave limit, for models of this type). It is neglected for simplicity and to emphasize the effect of the upwelling–downwelling nonlinearity as cleanly as possible.

The subsurface temperature, T_{sub}, is parameterized on the thermocline depth departure from its no-motion value, such that a deeper thermocline yields warmer temperatures of the water being upwelled. For the equatorial band SST equation, only the equatorial value of the thermocline depth departure, h_e, is required. An analytic function for this dependence is used:

$$T_{sub} = T_{s0} + (T_0 - T_{s0}) \tanh\left(\frac{h_e + h_0}{H^*}\right), \quad (2.5)$$

such that T_{sub} cannot exceed T_0 and cannot go below $T_0 - 2(T_0 - T_{s0})$. This provides a physically realistic nonlinearity and, with the upwelling–downwelling nonlinearity, guarantees that SST anomalies will remain bounded. Here T_{s0} is the temperature at an offset $-h_0$ from the thermocline, say 20°C, where h_0 controls the asymmetry of the thermocline depth dependence and H^* controls the maximum rate of change. Positive h_0 is appropriate since it gives a larger T_{sub} dependence on h_e when the thermocline is shallower than its average value. Values were chosen to give reasonable sensitivity of temperature to thermocline depth anomaly in the eastern part of the basin. The parameterization (2.5) is used for total h_e departure from its rest value and employs an analytic function to ensure nice properties of the phase space flow; it is not expected to give as good fit for interannual anomalies as the Zebiak and Cane (1987) parameterization from which it was inspired. Their version, however, suffers from the drawback that the Jacobian of the flow is undefined at the climatology, and our concern here lies more with qualitative properties than the exact amplitude of the anomalies.

The currents and thermocline perturbations are governed by linear dynamics, with contributions from two components,

$$w = w_s + w_m$$
$$u = u_s + u_m$$
$$v = v_s + v_m, \quad (2.6)$$

with subscript m representing the contribution at the surface of the vertical mean currents above the thermocline and subscript s representing the contribution of vertical shear currents associated with the fixed-depth surface layer. The vertical mean component is governed by shallow-water dynamics. In the fast-wave limit, these contributions are small and the approximation

$$u_m = v_m = w_m = 0 \quad (2.7)$$

is used. The vertical shear currents are governed by steady equations dominated by damping due to interfacial stress between the layers of damping time ϵ_s^{-1}, following Zebiak and Cane (1987). Only the values affecting the equatorial band are required; these are

$$u_s = b_u \tau$$
$$w_s = (-b_w + H_1 b_u \partial_x)\tau$$
$$v_N = -b_w L_y (2H_1)^{-1} \tau, \quad (2.8)$$

where $b_u \approx H_2/H_1\epsilon_s$ and $b_w \approx (H_1\beta/\epsilon_s)b_u$, where $H_2 = H - H_1$ is the depth of the second layer. Here u_s, w_s now denote equatorial values within the box and the meridional currents at the boundary of the box, v_N, have been evaluated from the continuity equation:

$$2\frac{v_N}{L_y} = \frac{w}{H_1} - \partial_x u.$$

In the fast-wave limit, the thermocline height along the equator, h_e, is in Sverdrup balance to a good approximation:

$$g\partial_x h_e = \tau, \quad (2.9)$$

where g is the reduced gravity parameter for the shallow-water ocean. In integral (dimensional) form,

$$h_e = h_E - g^{-1}\int_x^{x_E} \tau(s)\,ds, \quad (2.10)$$

where h_E is the thermocline depth anomaly at the eastern coast. In a finite basin, the specification of h_E is potentially important since it contains all the information about the boundary conditions and the effects of wave dynamics. For most of the runs discussed here, the following boundary condition for (2.9) is used, which applies when the meridional scales of the wind stress are sufficiently large compared to ocean damping (in dimensional form):

$$h_E = g^{-1}\int_{x_W}^{x_E} \tau(s)\left(\frac{s}{L}\right)^{1/2} ds, \quad (2.11)$$

where $L = x_E - x_W$ is the basin length. The effects of alternate versions of the boundary conditions are discussed with the derivation below. Equations (2.10) and (2.11) provide all the necessary information from the shallow-water component of the system since the thermocline height along the equator is what is required

for the SST equation and since vertical mean currents are small. The y dependence of the ocean fields could be generated diagnostically if desired. It is emphasized that (2.11) includes the net effects of equatorial adjustment in the x–y plane, which results in east–west asymmetry due to the β effect.

2) Derivation of the ocean boundary condition

The vertical-mean motions above the thermocline are governed by the shallow-water equations in the longwave approximation. In nondimensional form, with zonal distance scaled by the basin width, L, and meridional width scaled by the oceanic radius of deformation, L_D, but with time scaled appropriately for coupled SST evolution, these are

$$\begin{aligned}(\delta\partial_t + \epsilon)u_m - yv_m + \partial_x h &= \tau \\ yu_m + \partial_y h &= 0 \\ (\delta\partial_t + \epsilon)h + \partial_x u_m + \partial_y v_m &= 0, \end{aligned} \tag{2.12}$$

where δ is the relative adjustment time coefficient, which measures the ratio of the time scale of oceanic adjustment (in the zonal direction) by wave dynamics to the time scale of adjustment of SST by coupled feedback and damping processes. In the most physically realistic part of parameter space, δ is of order unity [see Neelin and Jin (1993) for a detailed scaling]. The fast-wave limit is defined by $\delta \to 0$, in which the wave dynamics time scales are fast compared to the coupled time scales affecting SST. Oceanic dissipation processes are represented by the damping time scale ϵ^{-1}, which is fairly long, so that $\epsilon \ll 1$ is a useful approximation; $\epsilon = (250 \text{ days})^{-1}$ yields nondimensional $\epsilon = 0.25$.

For simplicity, the case where zonal wind stress has a fixed y structure is taken. Consider first the case where the wind has an exponential (oscillatory and/or growing) time dependence, as for a linear coupled mode:

$$\tau^x(x, y) = e^{\sigma t}\tau_e(x)Y(y),$$

where $Y(y) = e^{-\alpha y^2}$. The Gaussian y dependence is simply a means of assessing the effects of meridional structure in the stress field, which prove to be secondary. The meridional length scales of the atmosphere, $L_a \approx 10°$, on the order of the atmospheric radius of deformation, are much larger than the oceanic radius of deformation, $L_D \approx 3°$, so that $\alpha = L_D^2/(2L_a^2) \sim 0.05$, even smaller than ϵ.

For this time dependence, we define $i\phi = \delta\sigma + \epsilon$. As the fast-wave limit is approached, that is, for frequencies and growth rates small compared to the inverse of the Kelvin wave crossing time, the ocean comes into balance to $O(\phi^2)$ in thermocline depth and $O(\phi)$ in currents, which can be driven by the small wind stress curl. Thus, the weak zonal currents are $O[\max(\phi,\alpha)]$, while at the equator the Sverdrup balance (2.9) holds locally to $O[\max(\phi^2,\phi\alpha)]$ for thermocline depth.

For the boundary condition on (2.9), the results of Cane et al. (1990) can be employed. The response of the shallow-water ocean at the eastern boundary, for wind stress of the assumed form, is

$$h_E = e^{\sigma t}\int_0^1 \frac{\tau_e(s)\sin 2\phi s}{(\alpha\cos 2\phi s + i\sin 2\phi s)^{1/2}}\,ds\left(\frac{i}{\sin 2\phi}\right)^{1/2}. \tag{2.13}$$

This expression can be sensitive to the order in which limits are taken [see Cane and Sarachik (1981)], but the fast-wave limit ($\delta \to 0$) is well defined in a physically appropriate manner by keeping finite damping or letting damping go to zero only after taking other limits. Equation (2.13) can be used as is but simplifies for $\epsilon^2 \ll 1$ (without yet making assumptions about the relative size of ϵ and α) to

$$h_E = \int_0^1 \tau_e(s)\frac{s}{\left(s + \dfrac{\alpha}{2\epsilon}\right)^{1/2}}\,ds. \tag{2.14}$$

When the atmospheric response has much larger meridional scale than the SST perturbation, that is, for $\alpha/2\epsilon \ll 1$, the second term in the denominator can be neglected, leading to the simplified form (2.11).

Numerical runs using (2.13) or (2.14) with various values of α and ϵ show very similar flow regimes to those obtained using (2.11). Two such figures are shown in the brief reply by Neelin et al. (1992b), which correspond to Figs. 4 and 5 of this paper but use (2.14) with $\alpha/(2\epsilon) = 0.1$ (corresponding, for instance, to oceanic damping time 250 days and atmospheric meridional scale 10°) instead. The features are almost identical. For larger values of $\alpha/(2\epsilon)$, some quantitative changes may be noted but the qualitative behavior is

TABLE 1. Standard parameter values.

Parameter	Symbol	Value
Atmospheric model amplitude factor	A*	0.05 Pa K^{-1}
Surface-layer coefficient	δ_s	1.0
Atmospheric damping	ϵ_a	(6000 km)$^{-1}$
Damping time for shear current	ϵ_s^{-1}	2 days
SST damping rate	ϵ_T^{-1}	180 days
Reduced gravity parameter	g	2×10^{-2} m s^{-2}
Offset parameter in T_{sub}	h_0	30 m
Sensitivity parameter in T_{sub}	H^*	50 m
Depth of layer above thermocline	H	200 m
Depth of surface layer	H_1	50 m
Depth scale for vertical advection	$H_{1\,1/2}$	100 m
Radiative-equilibrium SST	T_0	30°C
Off-equatorial SST	T_N	30°C
Temperature at no-motion thermocline	T_{so}	22°C

the same. Thus, for the figures presented here, (2.11) is used.

All of the above versions of the boundary condition contain the effects of equatorial wave dynamics on the adjusted ocean (although by definition the wave time scales are too fast to be important). It is of interest to test the effects of an alternate boundary condition that ignores the east–west asymmetry introduced by Kelvin and Rossby waves. The very simplest boundary condition is one of mass balance across the basin. The zonal mean over the basin of the thermocline depth departure from the no-motion level is forced to be zero; that is, no net mass is transported onto or off the equator. Away from the fast-wave limit, in regimes where wave time scales are important, this would be an important effect. In the fast-wave limit, the impact tends to be modest. Discussion of the results from this alternate boundary condition is given in section 4a.2 in the flow regime where it should have the greatest impact.

c. *Climatological state and coupling*

A smooth function that resembles the observed wind stress of the Pacific along the equator is used to set up the basic state,

$$\bar{\tau} = \frac{0.06Pa}{\rho H}\left\{0.12 - \cos^2\left[(x - x_0)*\frac{\pi}{2x_0}\right]\right\}, \quad (2.15)$$

with $x_0 = 0.57L$. The ocean basic-state variables, $\bar{T}$, $\bar{T}_{sub}$, $\bar{w}$, $\bar{v}_N$, and $\bar{h}$, are obtained from (2.4), (2.5), (2.8), and (2.10)–(2.11) with $\bar{\tau}$ given. The basic-state SST, vertical velocity, and thermocline depth departure are shown in Fig. 1 for standard parameter values. The SST has a very strong cold tongue in the eastern basin, with a shallow thermocline and strong upwelling region on and to the west, which resembles the observed climatology of the tropical Pacific to a reasonable extent.

The coupled system is set up using one-way flux correction, with wind stress given by

$$\tau = \tau' + \bar{\tau}, \quad (2.16)$$

where τ' is derived from the atmospheric response to SST anomalies,

$$T' = T - \bar{T}. \quad (2.17)$$

There is thus always a climatological stationary state, $\tau' = 0$, $T' = 0$ in both linear and nonlinear cases. For sufficiently small μ, the coupled system always decays to this climatological basic state at a rate given by a combination of the damping term in the SST equation and damping effects due to basic-state upwelling. At zero coupling, the constructed climatological state is thus unique.

The only respect in which the ocean model as used for the climatology and perturbations differs is that it is convenient to introduce a relative surface-layer coefficient δ_s that affects only the anomalous surface-layer currents. These can thus be reduced or even turned off to examine their effects without affecting the climatology. Thus, (2.8) is modified to

$$w = \bar{w} + \delta_s(-b_w + H_1 b_u \partial_x)\tau'$$
$$v_N = \bar{v}_N - \delta_s b_w L_y (2H_1)^{-1}\tau'. \quad (2.18)$$

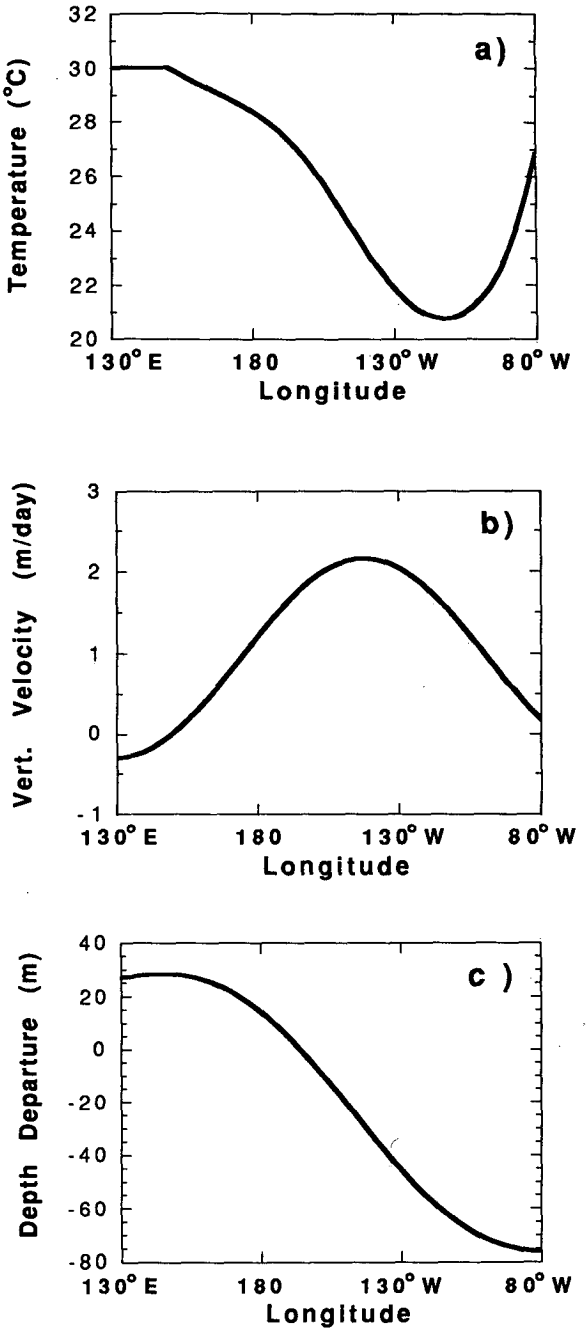

FIG. 1. The basic state of the tropical Pacific Ocean along the equator as used in the model: (a) Sea surface temperature (°C); (b) vertical velocity (m day^{-1}); and (c) thermocline depth departure from no-motion state (m).

To summarize, the coupled system consists of the SST equation (2.4), with subsurface temperatures, surface-layer currents, and equatorial thermocline depth given by (2.5), (2.18), and (2.10)–(2.11), respectively, plus the atmospheric model (2.2) or (2.3) coupled using the definitions (2.16)–(2.17). Standard values of the parameters are given in Table 1.

3. Linear analysis

For the model linearized about the climatological mean state of section 2b, the zonal eigenvalue problem is considered in a finite basin. A time-dependence $\exp(\lambda t)$ is assumed, and a simple matrix eigenvalue problem in x is obtained with the same finite differencing used in the nonlinear model. Typically, 40 to 50 points in x are sufficient for convergent results for the gravest modes.

Before discussing the finite-basin results, it is useful to summarize the periodic-basin case of N91. Several mechanisms, each corresponding to a term of the SST equation but with atmospheric feedback, contribute to growth of the SST modes. The dependence of these terms on zonal wavenumber differs but tends to favor the gravest modes for a basin of Pacific size. The mechanisms differ in tending to give eastward or westward propagation. The thermocline depth term tends to give eastward propagation. Consider a region of warm SST anomaly; it generates an eastward wind stress anomaly over and to the west of the region and a weaker westward stress anomaly to the east. The stress anomalies are balanced in the ocean by thermocline gradients in the fast-wave limit; these lead to a deeper thermocline below and to the east of the warm SST anomaly and a shallower thermocline to the west. With upwelling prevailing in the basic state for most of the basin, a region of deeper thermocline will result in warmer subsurface temperatures being upwelled to the surface and thus produce a warming tendency that occurs partly in the region of the original SST anomaly, reinforcing it, and partly to the east. A cooling tendency occurs in the shallower thermocline region to the west. For cold SST anomalies, the same applies with the sign reversed. Thus, a succession of warm and cold SST anomalies move eastward, amplifying if the reinforcing tendency due to coupled processes overcomes the damping terms.

On the other hand, surface-layer terms tend to give westward propagation. Enhanced (reduced) upwelling cools (warms) SST locally. Over and to the west of a warm anomaly, the westerly wind stress anomaly tends to reduce the upwelling anomaly, thus producing a warming tendency. Similarly, cold anomalies have easterly anomalies over and to the west of the region, yielding increased upwelling and cooling. A pattern of warm and cold SST anomalies is thus reinforced and moves westward. Zonal advection can have a similar effect. When both surface-layer terms and thermocline feedback occur, the growth tendencies add but the direction of propagation depends on which effect is stronger.

In a finite basin, similar effects occur, but the problem includes the effects of boundary conditions on the basin, and the modes will have more complicated spatial structure. Eigenvalues and eigenvectors of the most unstable mode(s) are examined in the following since these will determine the weakly nonlinear behavior in some neighborhood of the bifurcation from the climatological state. The value of the relative coupling coefficient, μ, is chosen such that the growth rate of the most unstable mode for each δ_s is close to zero (small positive), that is, that each case is just above the first bifurcation.

a. Dependence on the relative surface-layer coefficient, δ_s

Figure 2 shows eigenvalues and the corresponding SST eigenvectors for the most unstable mode(s) for different values of the relative surface-layer coefficient δ_s. Oscillatory modes have a complex conjugate pair of eigenvalues and eigenvectors that contain duplicate information; the real and imaginary parts of one eigenvector are given as a function of longitude, where the eigenvector corresponding to positive (negative) frequency is displayed for westward (eastward) propagating cases. For pure growth modes (a single real eigenvalue), the normalized eigenvector is pure real. In all cases, the eigenvectors are normalized such that the maximum SST amplitude has unit value. In two cases (Fig. 2b,c), the second most unstable mode is plotted as well.

As δ_s goes from the best estimate 1.0 to zero, the most unstable mode changes from a westward-propagating oscillatory mode to a stationary, pure-growth mode and then to an eastward-propagating oscillatory mode. This transition may be qualitatively anticipated from the periodic-basin case except that stationarity occurs only for an infinitesimal range of δ_s. The periodic case gives no information of the change of structure since zonal wavenumber is fixed, but it does show that for smaller zonal wavenumbers, the thermocline feedback term is more important, so the transition occurs at larger δ_s. The periodic case also predicts that higher coupling will be required to destabilize a given mode when the surface-layer feedbacks are weaker.

Two obvious differences arise in the basin case. First, the zonal structure of the modes is internally determined, with the boundary conditions yielding quantized modes and a combination of zonal variation in the basic-state parameters and east–west asymmetry due to β yielding east-basin trapping (see JN for details). Second, one of the modes is stationary over a very considerable range of parameters. This mode changes very slowly from Fig. 2b to Fig. 2e, but in the latter it has acquired a very small imaginary part as-

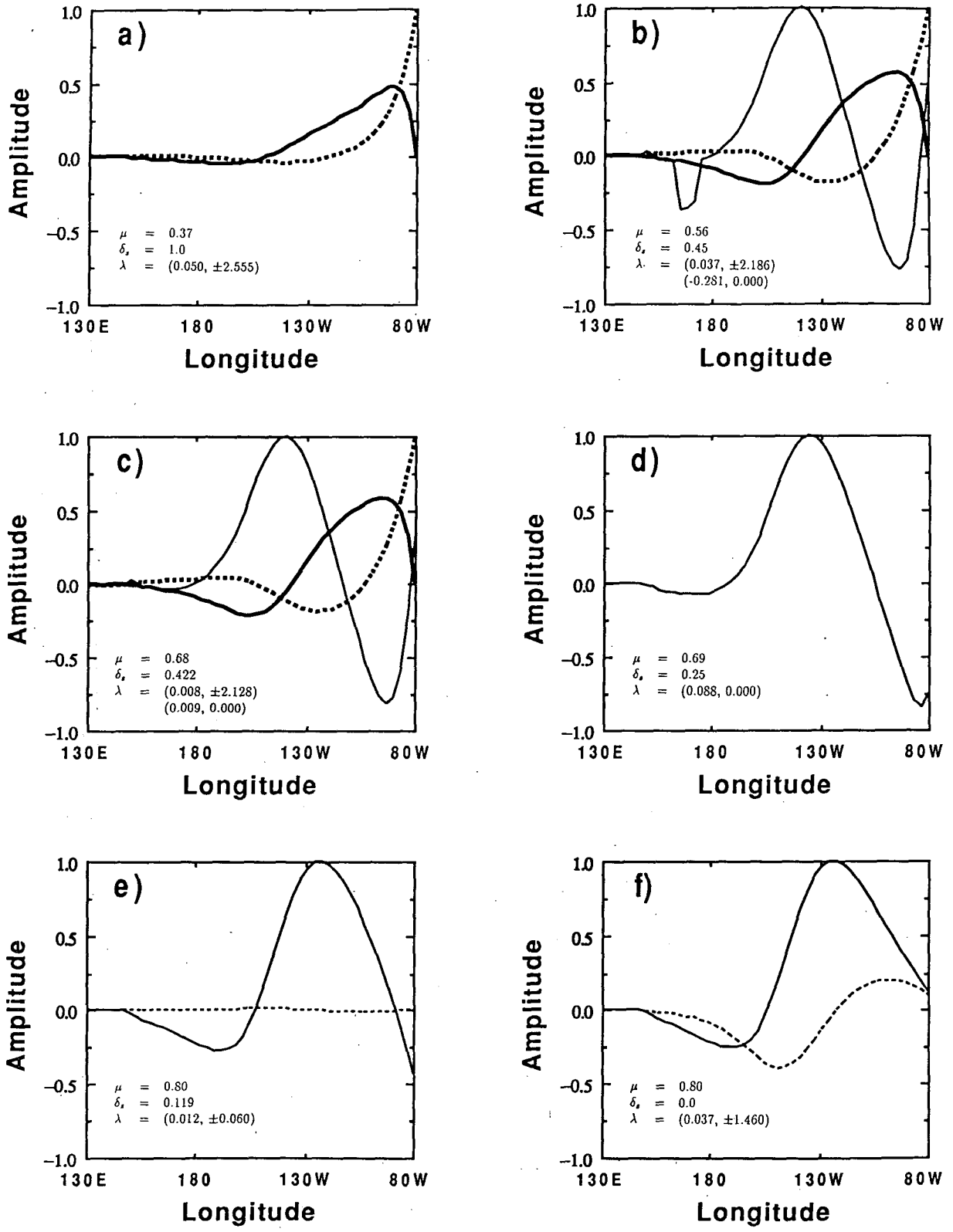

FIG. 2. Eigenvectors of SST and eigenvalues for the most unstable mode (or two most unstable modes) for various values of the surface-layer coefficient δ_s as indicated. Solid (dashed) lines: real (imaginary) part of SST eigenvector (nonoscillatory modes have only real part). Heavy lines correspond to westward-propagating oscillatory mode. Light lines correspond to stationary or eastward-propagating mode. Eigenvalues, λ, are given as (growth rate, frequency) in per year. Periods corresponding to the frequency are (a) 2.45 yr; (b) 2.87 yr; (c) 2.95 yr; (d) ∞; (e) 104.72 yr; (f) 4.30 yr. The atmospheric damping length, ϵ_a^{-1}, is 6000 km.

sociated with the transition to eastward propagation. The mode has both a standing component and an eastward-propagating part in both Figs. 2e and 2f, with the eastward propagation giving the frequency. The transition occurs at a degeneracy of algebraic multiplicity 2 (abbreviated here as "2-degeneracy"), where two eigenvalues become identical at a singularity in the parameter space. For higher δ_s, these correspond to the unstable stationary mode shown and a faster-decaying stationary mode that combines with it at the 2-degeneracy to give a complex pair.

A similar 2-degeneracy can arise at large δ_s, where the stationary mode can undergo a transition to westward propagation, as discussed in JN. In addition, a different effect, not pursued by JN, is found here, in that two distinct modes vie for dominance: at larger δ_s, the westward-propagating mode of Fig. 2a has the largest growth rate by a considerable margin; at lower δ_s, the mode of Figs. 2d–f, either in its stationary or eastward-propagating version, is faster growing. These two SST modes are simply different zonal modes—essentially the gravest and second gravest spatial modes. Both have comparable wavenumbers in terms of zero crossings, but the westward-propagating mode has larger effective complex wavenumber due to the strong exponential trapping toward the eastern side of the basin.

For intermediate values of δ_s, both modes have comparable growth rates. Figure 2c shows a case, near $\delta_s = 0.422$, where both modes go unstable simultaneously in a codimension 2 bifurcation. In such instances, one anticipates the complexities associated with Hopf–steady state mode interaction (Golubitsky et al. 1988). The location of this region where both

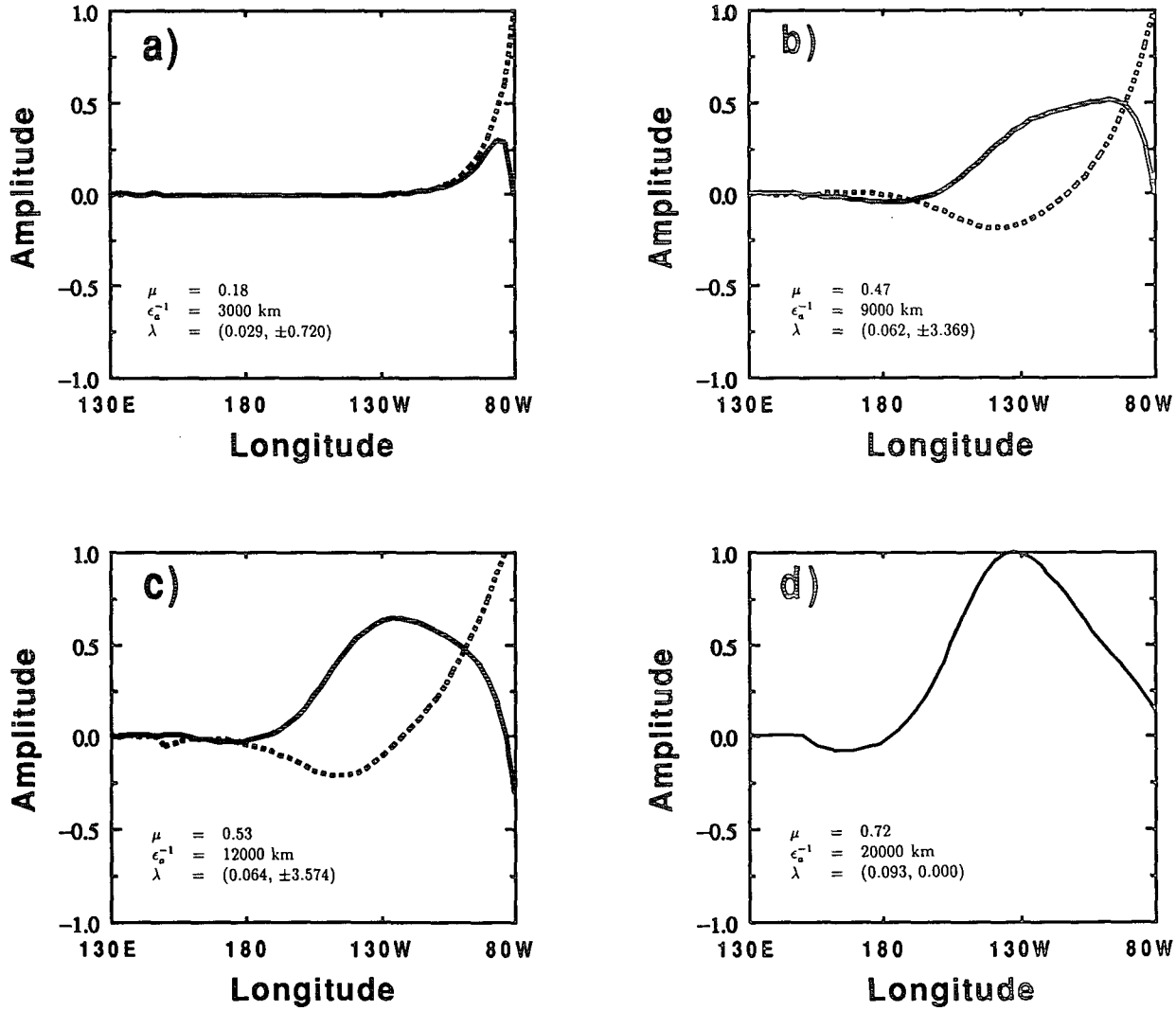

FIG. 3. Eigenvectors of SST and eigenvalues for the most unstable mode for various values of the atmospheric damping length, ϵ_a^{-1}, as indicated. (a)–(c) Surface-layer coefficient 1.0, may be compared with Fig. 2a but using damping lengths of 3000, 9000, and 12 000 km, respectively. (d) Surface coefficient 0.0, may be compared to Fig. 2f but using damping length 20 000 km. Other conventions as in Fig. 2. Periods corresponding the frequency are (a) 8.73 yr; (b) 1.86 yr; (c) 1.76 yr; and (d) ∞.

modes coexist with comparable growth rate will shift somewhat as other parameters, such as ϵ_a, are varied, but appears to be a fairly robust feature.

b. Dependence on atmospheric damping

The atmospheric damping parameter, ϵ_a, an inverse damping length scale, is used here as a measure of the sensitivity to changes in the atmospheric structure. It has two primary effects: 1) as it becomes larger, the atmospheric response becomes more local, so that finite-basin effects in the atmosphere become less important, and 2) it affects the relative phase of the wind and SST (see N91 for a discussion in the periodic case).

In the case of $\delta_s = 1$, the unstable westward-propagating mode has no qualitative change as a function of ϵ_a. Figures 3a,b,c, showing both longer and shorter damping lengths, may be compared to Fig. 2a. For larger ϵ_a, however, the modes tend to be trapped more to the eastern coast and have a longer period.

For the case of zero relative surface-layer coefficient, that is, where the surface layer is inactive and coupling is governed by the thermocline feedback, the unstable mode was eastward-propagating in Fig. 2f but can be stationary for many choices of the atmospheric damping length. Figure 3d shows this mode and its associated eigenvalues near the bifurcation for $\epsilon_a = (20\,000\ \text{km})^{-1}$. The interpretation is simply that the same 2-degeneracy surface encountered for δ_s near that of Fig. 2e is crossed by changing ϵ_a between the cases of Fig. 2f and Fig. 3d. The SST anomaly is nearly all of a single sign when the damping length, ϵ_a^{-1}, is large, more closely resembling the SST anomalies found in the Cane and Zebiak (1985) model, but this does not fundamentally affect the properties of the mode.

4. Nonlinear cases

A feeling for the variety of flow regimes that can occur in this model and the possible relation of these to other models or to the observed system can be obtained by simple forward time integration. In this

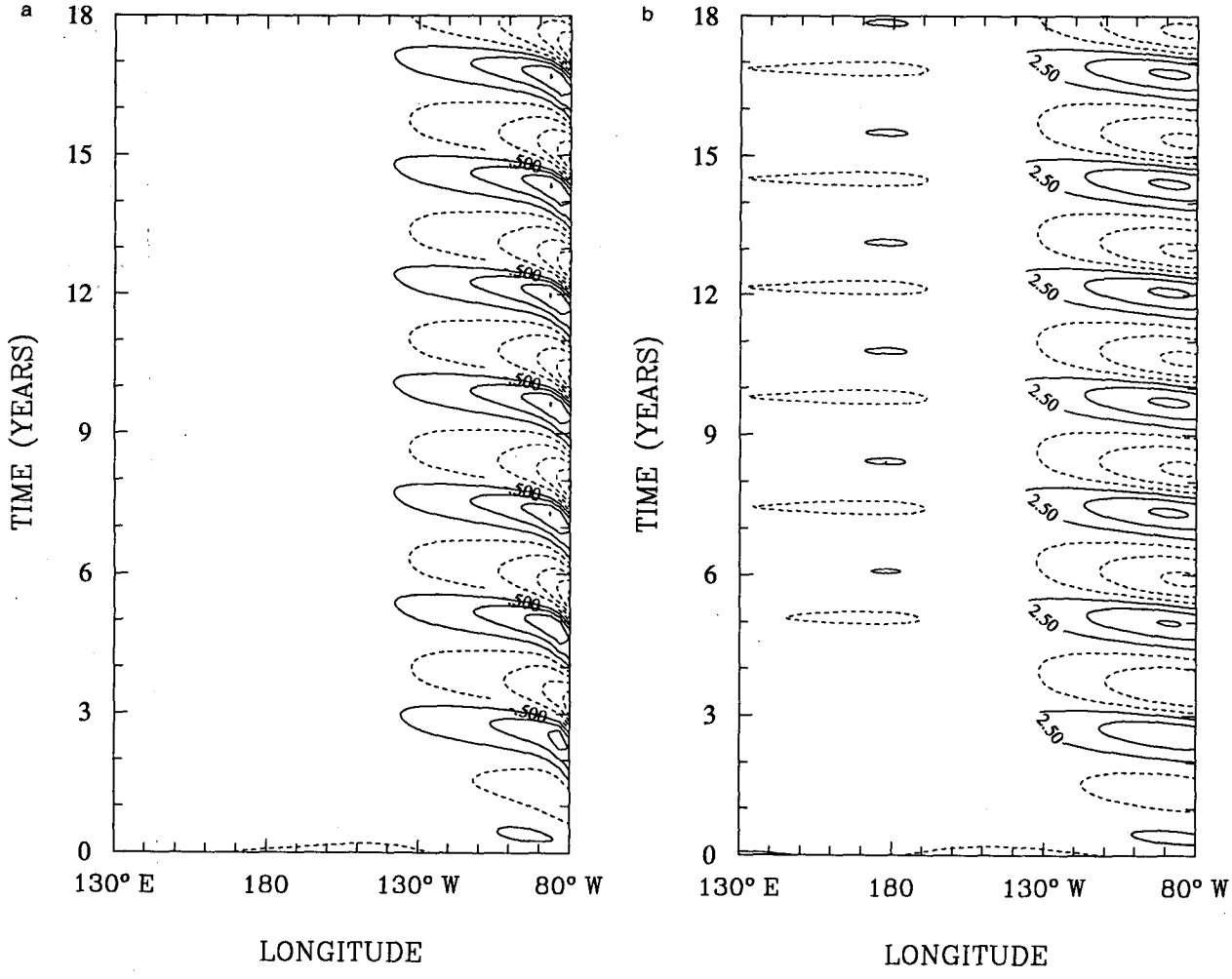

FIG. 4. Time–longitude diagram of a 18-year run of the nonlinear model with $\delta_s = 1$ and $\mu = 0.37$. (a) SST anomaly (contour interval 1.0°C) and (b) thermocline depth anomaly (contour interval 5 m). Solid (dashed) lines show positive (negative) contours.

model, the spatial dependence is well summarized by SST and thermocline depth anomalies along the equator, with upwelling anomalies described when appropriate. In large parts of parameter space, there is only a single attractor, and thus, the initial conditions are irrelevant to the long-term behavior. The spinup from initial conditions (consisting of SST anomalies of modest amplitude and the ocean circulation implied by these) is often shown since this short-term evolution sometimes provides an indication of other interesting behavior and gives an idea of the decay rate toward the attractor. Where multiple attractors (usually stationary points) exist, these are found by choosing initial conditions in the respective attractor basins, guided by physical considerations and information from neighboring parts of parameter space. Extended integrations and runs at intervening parameter values were used to ensure that the attractors were mapped with reasonable confidence for most of the cases presented. There are a few cases where more powerful techniques (e.g., Keller 1977) would be useful to give a complete understanding of the bifurcation diagram. Given that the continuity of the system in parameter and phase space dictates the linkage between regimes, however, the most important connections are usually obvious.

a. Weakly nonlinear cases

1) WESTWARD-PROPAGATING CASES

Figure 4 shows the nonlinear numerical results in the case of full surface-layer feedbacks, $\delta_s = 1$. The value of the coupling coefficient, μ, is chosen such that the flow is in the regime just above the first bifurcation point. The oscillation has a period of about 3 years, which is equivalent to the results of linear analysis. As expected for a supercritical Hopf bifurcation, this weakly nonlinear oscillation has the same form as the linear pair of eigenmodes at the bifurcation. From a small perturbation, the unstable mode grows until it equilibrates to the limit cycle shown. Below the bifur-

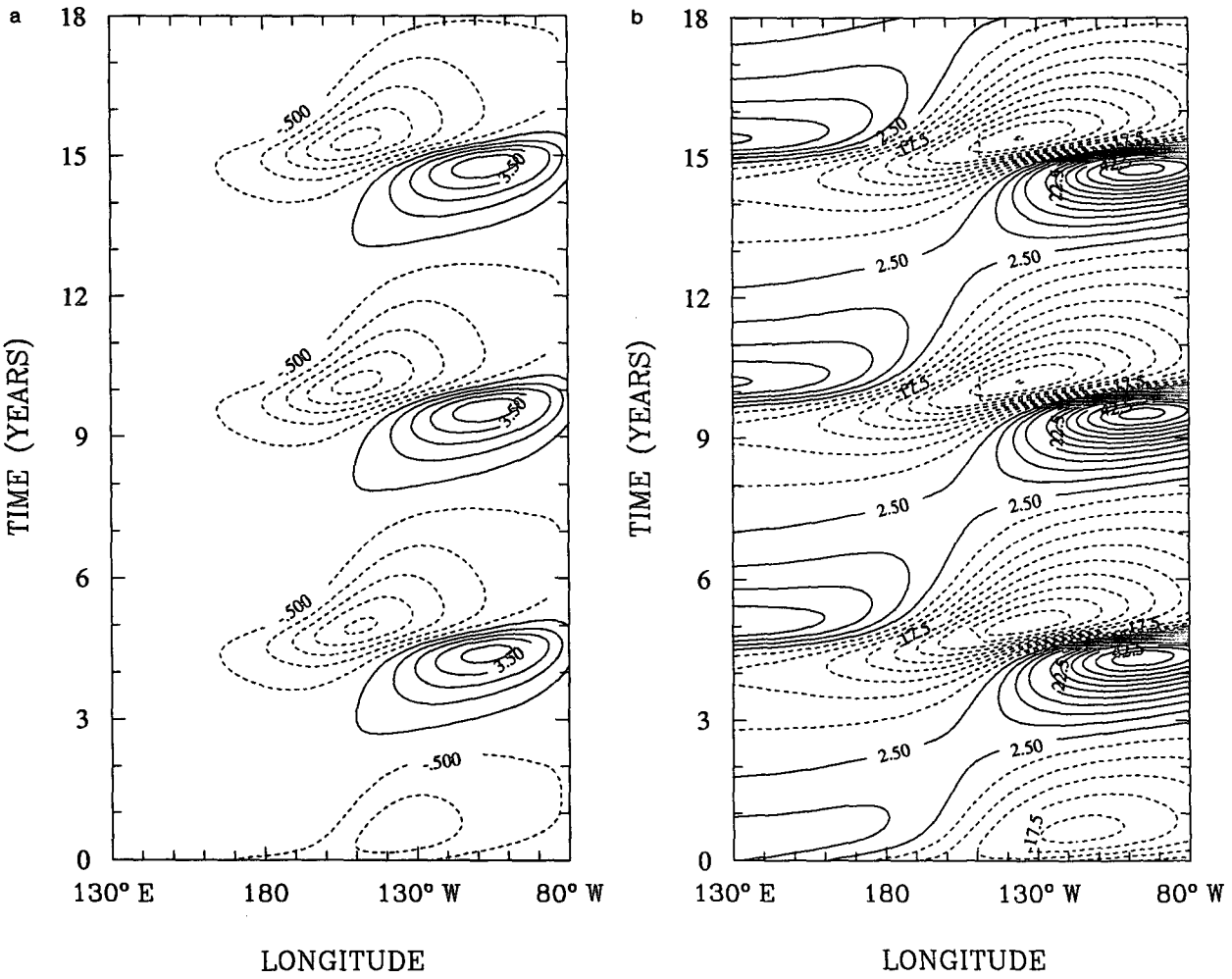

FIG. 5. As in Fig. 4 but for surface-layer coefficient $\delta_s = 0.0$ and $\mu = 0.8$: (a) SST anomaly and (b) thermocline depth anomaly.

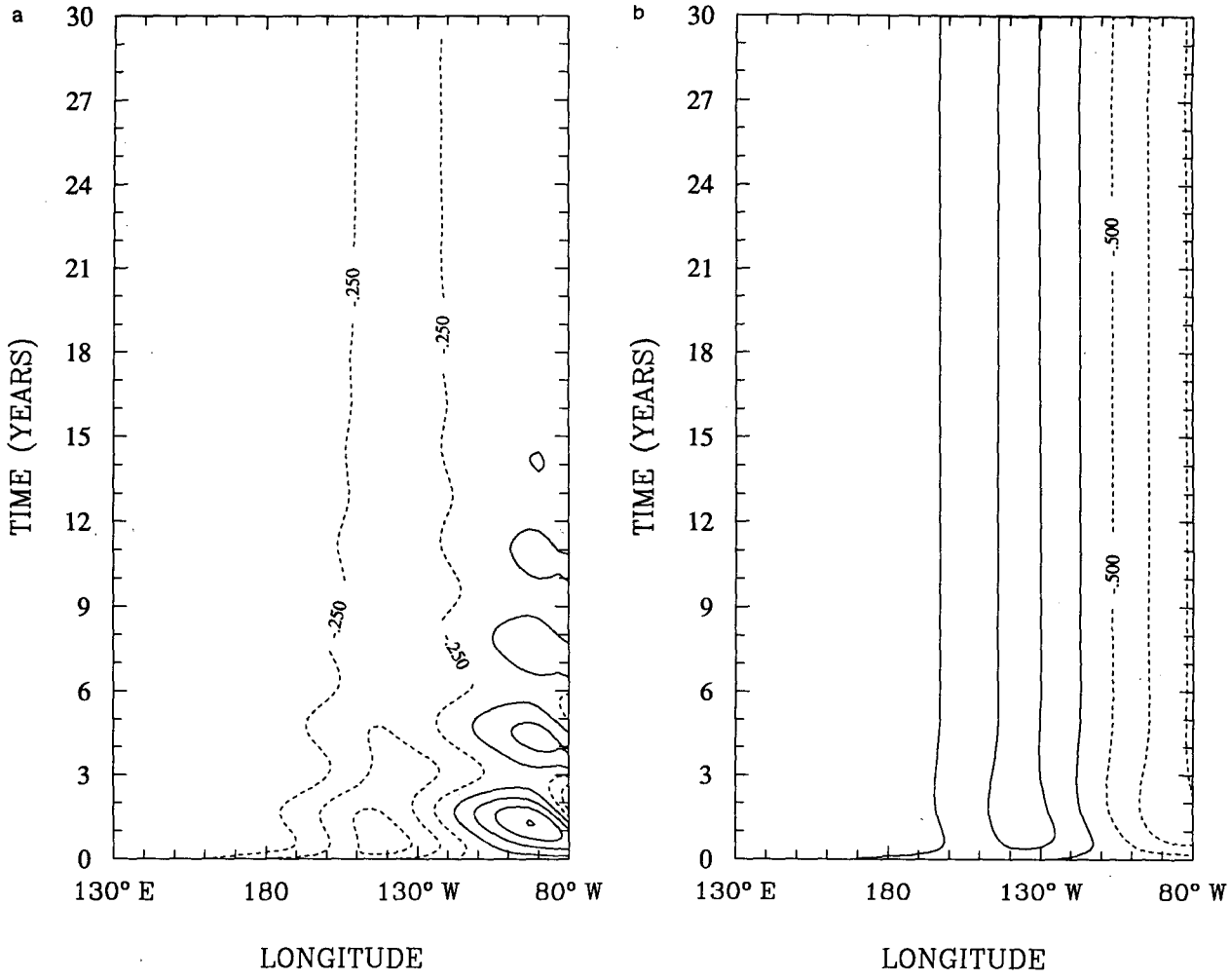

FIG. 6. Time–longitude diagram of SST anomaly for three 30-year runs of the nonlinear model with $\delta_s = 0.35$, $\mu = 0.673$ and from different initial conditions leading to the three stable stationary states: (a) cold state, (b) warm state, and (c) extreme warm state; otherwise, as in Fig. 4a.

cation, of course, the same oscillation decays slowly toward the climatological stationary point.

The SST anomalies are trapped in the eastern part of the basin and are westward propagating. Wind anomalies propagate coherently with the SST anomalies, with westerlies just to the west of warm SST producing downwelling and eastward surface current anomalies (not shown) in this region. Changing parameters has the same effects noted in the linear analysis; for instance, for larger atmospheric damping length, the SST anomalies extend farther westward into the basin. We suggest that the features of this oscillation provide a simple analog for westward-propagating oscillations found in some coupled GCMs (e.g., Meehl 1990; Lau et al. 1992) and for the westward-propagating features of the low coupling oscillation in the hybrid model of Neelin (1990a). Deep thermocline anomalies occur in the west preceding each warm phase; these are not large for the case shown but are more developed when the oscillation occupies more of the basin. The thermocline feedback does contribute to slowing the period of the oscillation but is not crucial to its form or existence.

While the effects of seasonal forcing are not examined here, it is often possible to frequency lock such nonlinear oscillations to the forcing period. In this case, a mode of this form would potentially provide an explanation for the westward propagation of zonal wind and SST found in the observed seasonal cycle (G. Philander, personal communication; Philander and Chao 1991).

2) EASTWARD-PROPAGATING CASE

Figure 5 shows the weakly nonlinear oscillation corresponding to the linear eastward-propagating mode of Fig. 2f, again through a supercritical Hopf bifurcation. For this case with no surface-layer current anom-

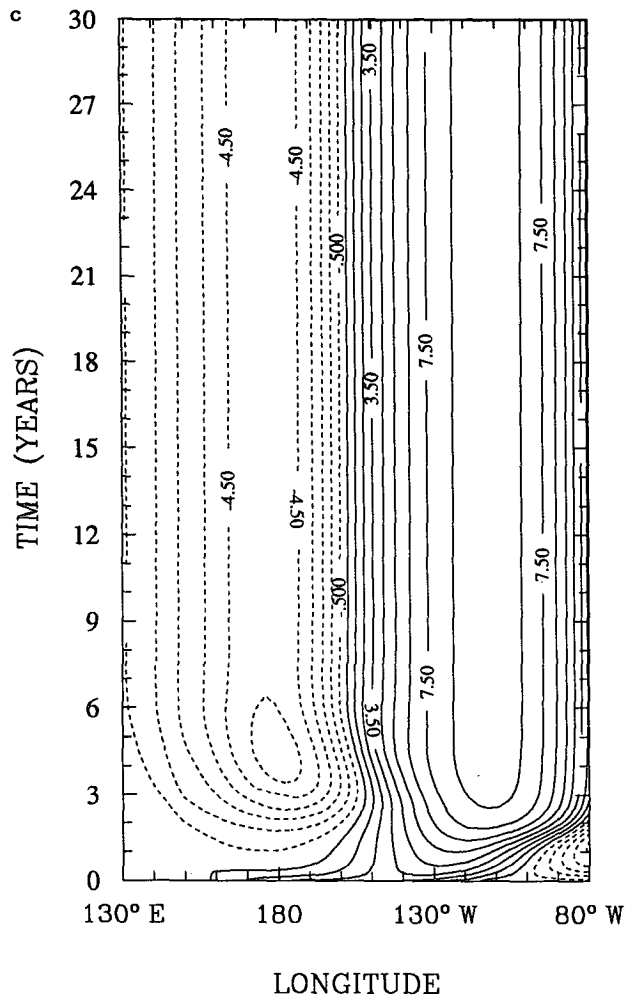

FIG. 6. (*Continued*)

alies, $\delta_s = 0$, and $\epsilon_a = (6000 \text{ km})^{-1}$, the mode has very slow eastward propagation that produces a 5-yr cycle. In addition to the propagating component responsible for the period, the SST anomaly has a very significant standing oscillation component. SST anomalies are trapped to the east of the date line as discussed in the linear case.

The thermocline in the west exhibits fairly large variations that lead the east in a manner similar to the observed and to that found in other models. Time delay in ocean dynamics is by definition, however, unimportant in this model. This phase relation is primarily a consequence of the Sverdrup balance with the boundary condition (2.11) playing an additional role. These features have some resemblance to the 1982–83 El Niño and provide an analog for a number of other simple coupled models such as Anderson and McCreary (1985), Yamagata and Masumoto (1989), and Yang and O'Brien (1993). They also closely resemble the oscillation found in Wakata and Sarachik (1991) despite the fact that wave time scales very likely play a role in that oscillation (JN).

To check the importance of the boundary condition (2.11), which contains the steady effects of wave adjustment processes on the slow solution, these runs were repeated using the simple mass-balance boundary condition. The results gave the same types of bifurcation (although not exactly for the same parameters) and similar features of the unstable mode, for example, trapping in the eastern part of basin and patterns of eastward propagation. This suggests that the oceanic boundary condition is not crucial factor for the qualitative behavior in this regime. Since this is a case dominated by the thermocline feedback, one would expect this to be the regime for which it would have greatest importance. Similar results were obtained for other regimes as well. Note, however, that JN found the wave-related boundary condition to be important to eastward trapping when there is no zonal variation in the basic state. When wave time scales are important, as in Cane et al. (1990), the eastern boundary condition plays a more significant role.

3) STATIONARY CASE

From the linear analysis, it is known that the unstable mode is stationary for some δ_s values between the cases of westward propagation and those of eastward propagation, or for larger values of the atmospheric damping length ϵ_a^{-1}. Figures 6a–b show the two stable stationary solutions corresponding to the linear unstable mode shown (for slightly different δ_s) in Fig. 2d. The decaying oscillation about the cold state that may be noted in

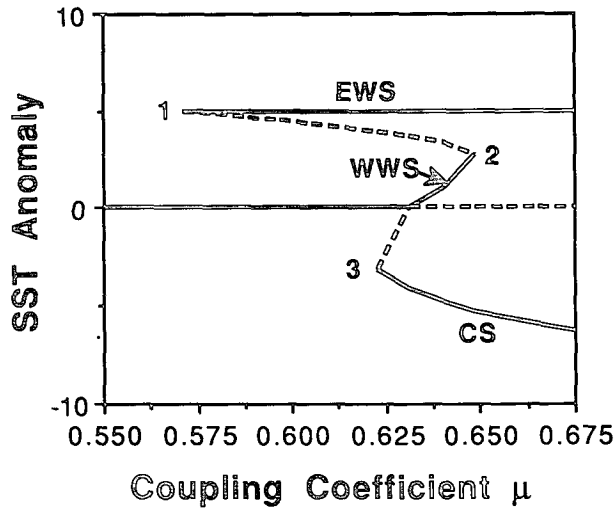

FIG. 7. Bifurcation diagram for the "toy" model with $\delta_s = 0.35$. Stable (unstable) stationary states are indicated by solid (dashed) lines, respectively. The extreme warm stationary state is marked EWS, the weak warm stationary state WWS, and the cold state CS, while the limit points are indicated by the numbers 1, 2, and 3.

Fig. 6a will be discussed further on. Since there is no symmetry between positive and negative anomalies for the nonlinearity present in this model, the generic stationary bifurcation is a transcritical bifurcation. This is confirmed by verifying that the cold state exists for values of μ smaller than the bifurcation, while the warm stationary state appears above the bifurcation.

The picture is complicated, however, by the presence of nearby bifurcations for each of the stationary solutions. The cold state shown here owes its presence above the transcritical bifurcation to a saddle-node bifurcation that redirects this branch toward higher coupling. The weakly nonlinear warm branch disappears for slightly larger μ, apparently in another saddle-node bifurcation. This is in turn associated with the presence of an additional, highly nonlinear stable stationary state. Figure 6c shows this extreme warm stationary state for the same value of μ as Figs. 6a, b. Physically, it is due to an almost complete "shutoff" of the upwelling. Additional runs indicate that this extreme warm stationary state exists and is stable even for values of μ smaller than those where the cold state exists; that is, its range extends to a lower, though still finite, value of coupling. For the stationary unstable mode that leads to the cold and weak warm stationary states, the thermocline feedback is an important source of instability, so the nonlinearity in the T_{sub} parameterization is important. Because of the basic-state thermocline slope, this is encountered at fairly small amplitude for cold anomalies in the eastern basin, limiting the magnitude of the cold stationary state.

This pattern, in which two or three stable stationary states coexist over different ranges, can be seen in a very simple context by considering a local-feedback model with the same nonlinearities in the SST equation. By assuming that oceanic vertical velocity, thermocline depth, and atmospheric wind stress anomalies are all proportional to the local SST anomaly, and keeping the same SST equation (2.4) and the same subsurface temperature parameterization (2.5), one obtains a "toy" coupled model that provides a close analog to this aspect of the bifurcation tree. Figure 7

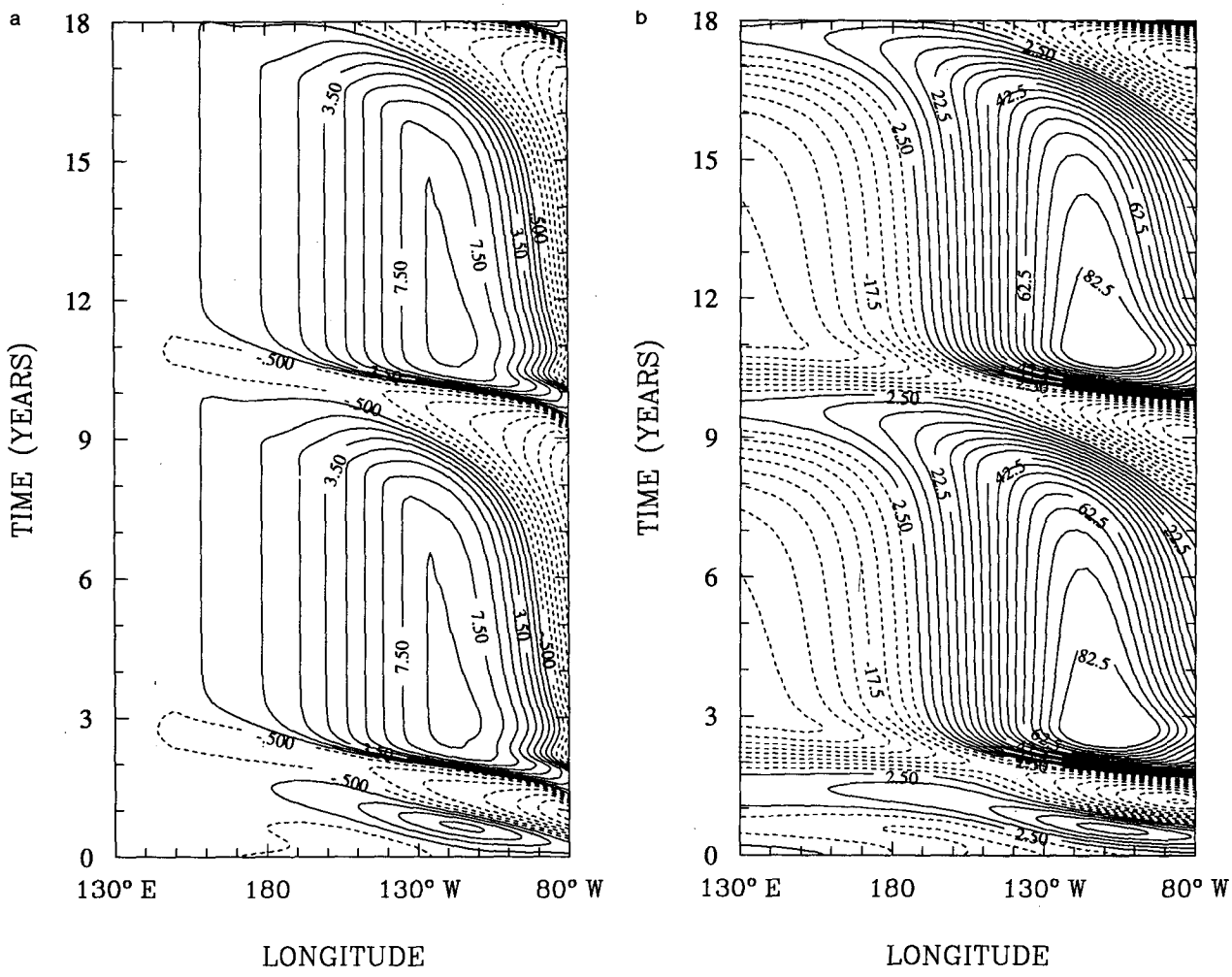

FIG. 8. As in Fig. 4 (strong surface-layer feedback) but for higher coupling, $\mu = 0.6$: (a) SST anomaly and (b) thermocline depth anomaly.

shows the stationary solutions of the toy system as a function of μ for $\delta_s = 0.35$. The value of h_0 in (2.5) has been reset to 10 m for the toy model to characterize the mean of the climatological depth across the basin plus the standard value of h_0. The large magnitude of the cold state (marked CS) is due to the fact that typical basinwide values are considered in the toy model, whereas the slope in the thermocline basic state in the full model results in strong nonlinearity being encountered quickly in the eastern basin. The mean thermocline depth departure from the no-motion level, $\bar{h}$, combined with the offset, h_0, in (2.5) is primarily responsible for the tilt of the transcritical bifurcation since it breaks warm–cold symmetry in the nonlinearity of the subsurface temperature, which is dominant for small anomalies and for the cold state. Upwelling nonlinearity tends to give an opposite slope.

The extreme warm state (EWS) is due to the upwelling–downwelling nonlinearity. For large warm anomalies, westerly wind anomalies reduce the upwelling; if coupling is strong enough, these can overcome the mean easterlies to shut off the upwelling altogether and create a downwelling state, thus maintaining the warm anomalies. The unstable branch connected to the EWS (at the saddle node bifurcation marked 1 on the diagram) has reduced upwelling but does not entirely overcome the mean upwelling. As the amplitude of this branch decreases, the increased upwelling produces greater importance for the thermocline feedback and the branch turns around at the limit point marked 2 to yield the stable, weak-amplitude warm stationary state (marked WWS). On the cold side of the transcritical bifurcation, this branch is unstable until it is redirected toward higher coupling by the saddle node bifurcation marked 3.

Three stable stationary states coexist in a very small range of μ (between the μ values at 2 and 3), associated with this trade-off between upwelling versus subsurface temperature nonlinearities. Naturally, two unstable stationary states exist between the three stable ones. Multiple stationary states exist for all coupling values greater than a certain threshold, but over most of the range there are two stable states and one unstable one, although which is unstable depends on being above or below the bifurcation from the climate state. Although the region in parameter space with three stable states is small, it is significant because it separates regions dominated by different dominant physical mechanisms for instability and hence different nonlinear terms. For very small δ_s, the extreme warm stationary state would not be encountered until much larger μ, while for small thermocline feedbacks, the transcritical bifurcation would slope the other direction.

b. Relaxation oscillations in strongly nonlinear cases

Relaxation oscillations are found over wide ranges of the coupled parameter space. To illustrate, two extreme cases were chosen: $\delta_s = 1$ and $\delta_s = 0$, which have westward and eastward propagation, respectively, at low coupling. Very close to the bifurcation, the oscillation at any given longitude would be purely sinusoidal. As coupling increases, asymmetry between the warm and cold phases arises as one of the two begins to lengthen, distorting the limit cycle into a relaxation oscillation.

1) WESTWARD-PROPAGATING CASE

Figure 8 shows a well-developed relaxation oscillation for $\mu = 0.60$, which may be compared to the $\mu = 0.37$ case in Fig. 4. The flow evolves very slowly during the warm phase, then passes relatively quickly through the cold phase whose length has not changed much relative to low coupling. The overall period thus increases dramatically with coupling: about 8 years for the case shown and approaching infinity for somewhat larger values. The westward propagation is by definition essential to the oscillation but is not as easily visible,

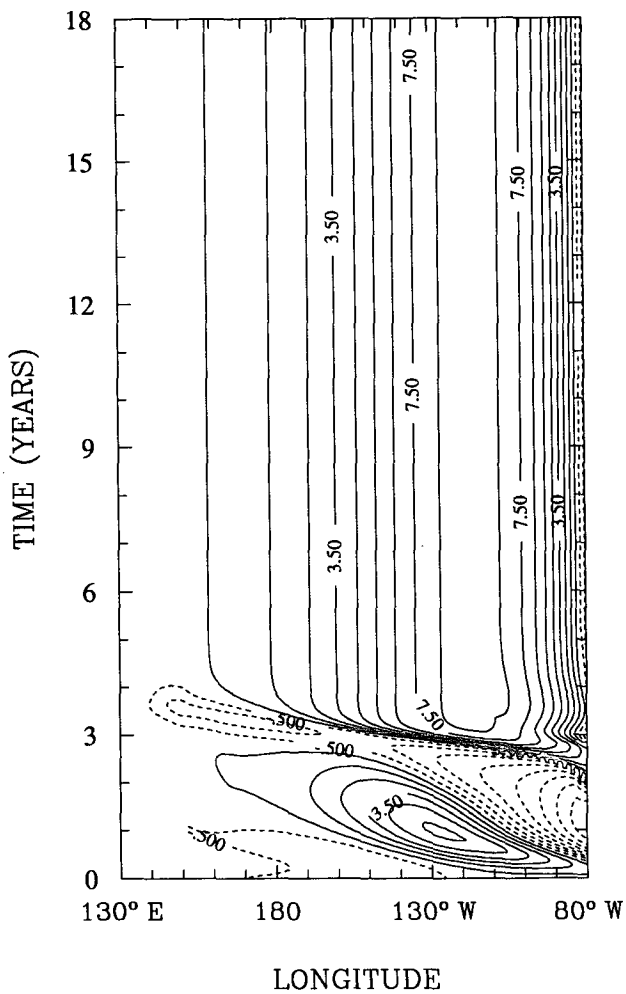

FIG. 9. SST anomaly as in Fig. 4a but for $\mu = 0.65$.

especially during the warm phase. There are even slight hints of eastward propagation in some areas just after the sudden establishment of the warm phase. The transition from cold phase to warm phase is very fast, and if finite wave time scales were included in the model, they would certainly have some effect during this phase while being unimportant to the very long period oscillation as a whole.

The picture shown here bears considerable qualitative resemblance to the oscillation found in the hybrid GCM of Neelin (1989a, 1990a). As in that case, the physical mechanism for the lengthening of the warm phase is associated with shutting off upwelling. During the warm phase, the strong downwelling anomaly produced by westerly winds overcomes the climatological upwelling and replaces it with near-zero or downwelling vertical velocity over large parts of the basin. The vertical–meridional advection loop is thus in a state where subsurface temperature has little effect on the equatorial SST, being replaced by off-equatorial temperatures that are little different than those at the equator during the warm phase. In this model, the upstream differencing scheme makes this explicit. Zonal advection likewise would have little effect since the zonal gradient has been wiped out over much of the basin. The flow in phase space thus becomes very slow. The instability that gave rise to this oscillation depends strongly on vertical velocity anomalies. It is thus natural that at strong coupling, it should encounter its limiting nonlinearity in this term. Since this strong upwelling–downwelling nonlinearity can be encountered only during a warm phase, it is the warm phase that participates in producing the relaxation oscillation.

Further increasing μ leads from this relaxation oscillation to a stable stationary solution, apparently in a global bifurcation. The first 18 years of a run with $\mu = 0.65$ are shown in Fig. 9. The stationary state, which has a very similar structure to the warm phase of the relaxation oscillation but with upwelling wiped out over almost the entire basin, remains constant for at least

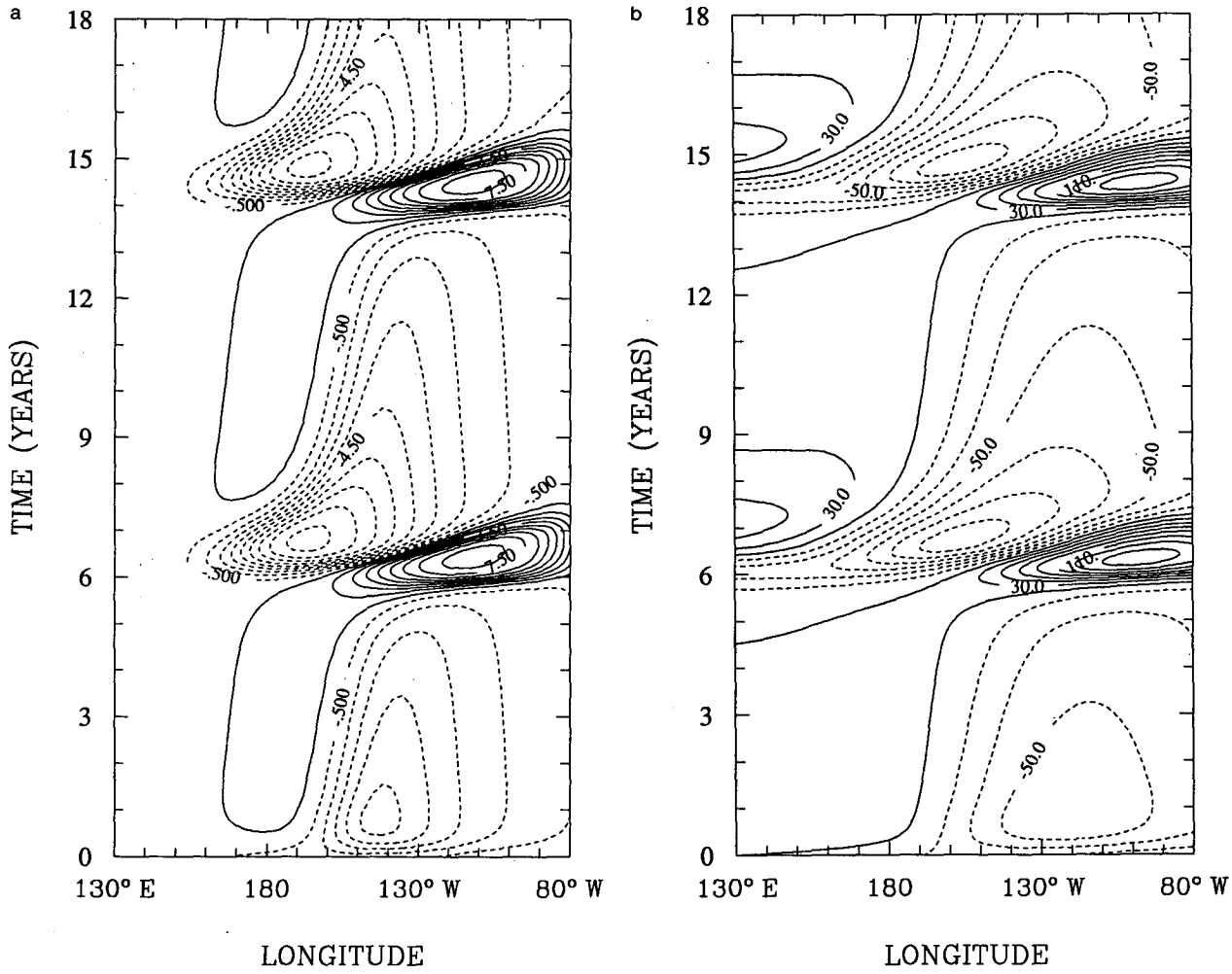

FIG. 10. As in Fig. 5 (no surface-layer feedback) but for high coupling, $\mu = 1.05$: (a) SST anomaly and (b) thermocline depth anomaly. Plotting conventions as in Fig. 4 except contour interval of 20 m in (b).

50 years. The simplest explanation is that the limit cycle encountered an unstable stationary point that lay between it and the stable stationary point and disappeared. For at least some parameter values, it can be confirmed that the stable stationary point can coexist with the relaxation oscillation, as was found in Neelin (1990b). The system for a smaller or larger ϵ_a shows similar relaxation oscillations.

2) EASTWARD-PROPAGATING CASE

The relaxation oscillation is also robustly present in the case that has an eastward-propagating oscillation at low coupling. Figure 10 shows an example for $\delta_s = 0$. In this case, the cold phase lengthens rather than the warm phase. The difference from the westward-propagating case is that the thermocline feedback is more important to the low-coupling instability mechanism than the surface-layer upwelling mechanism. The system thus first encounters strong nonlinearity in the T_{sub} term. This occurs during the cold phase since the basic state $\bar{h}$ is already shallow in the east. In a strong cold phase, further raising the thermocline in the east yields little additional reduction in the subsurface temperature being brought to the surface by upwelling. The vertical gradient between surface and subsurface temperature, which was the main source of SST change, has been greatly reduced over much of the basin, so the flow changes only slowly. Once warming begins in part of the basin, however, both vertical and horizontal gradients at the boundary are large, so the transition occurs very quickly.

Again, propagations of SST anomalies are essential to the oscillation but are not very obvious during large parts of the cycle. If noise were added to the system, it would be very difficult to deduce the source of oscillation simply by inspection of the anomalies. As in the westward-propagating case, as μ is further increased, the relaxation oscillation gives way to a permanent cold stationary-state solution (Fig. 11) that is very close to the cold phase of the relaxation oscillation.

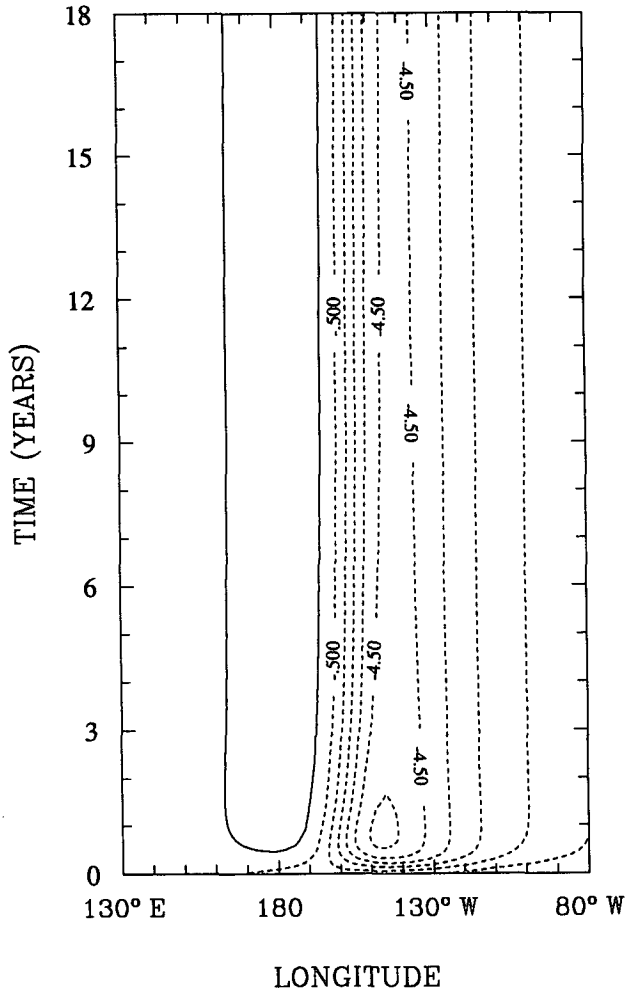

FIG. 11. SST anomaly as in Fig. 10a but for $\mu = 1.15$.

c. *Higher bifurcations for the case of intermediate δ_s*

The behavior of the coupled system is quite complicated for intermediate δ_s values where no single process dominates. For illustration, the case of $\delta_s = 0.35$ is chosen. This is in the region where the first bifurcation is associated with the stationary mode of Fig. 2d but is not too far away from the region (near $\delta_s = 0.422$) where both westward and stationary oscillations bifurcate simultaneously (Fig. 2c). Several points from a section in the μ direction in parameter space are shown, although some knowledge of the behavior in the neighboring δ_s range is necessary.

Section 4a.3 discussed the three stationary solutions for coupling values slightly above the first bifurcation point. Figure 12 shows the behavior for μ just slightly larger than the case of Fig. 6. The cold stationary state (Fig. 12b) is still stable, but a mode of oscillation about this state is only weakly decaying. The warm stationary state of Fig. 6a is either unstable or, more likely, no longer exists, and the system instead enters an extreme warm stationary state that is related to that of Fig. 6c, although the spatial form is somewhat different. This is consistent with the bifurcation diagram from the toy model; Fig. 12 would correspond to the region just after the limit point of the smaller amplitude warm stationary state, with the unstable branch joining the very warm stationary state at lower coupling through a second saddle-node bifurcation. It may be noticed that the phase-space flow is nonetheless slow in the region where the low-amplitude stationary point existed at lower coupling, and the system lingers there before reaching the high-amplitude state. The high-amplitude warm state shares some features with that found for larger δ_s in that the original climatological upwelling has been shut off, but there is perturbation upwelling in the west of the basin.

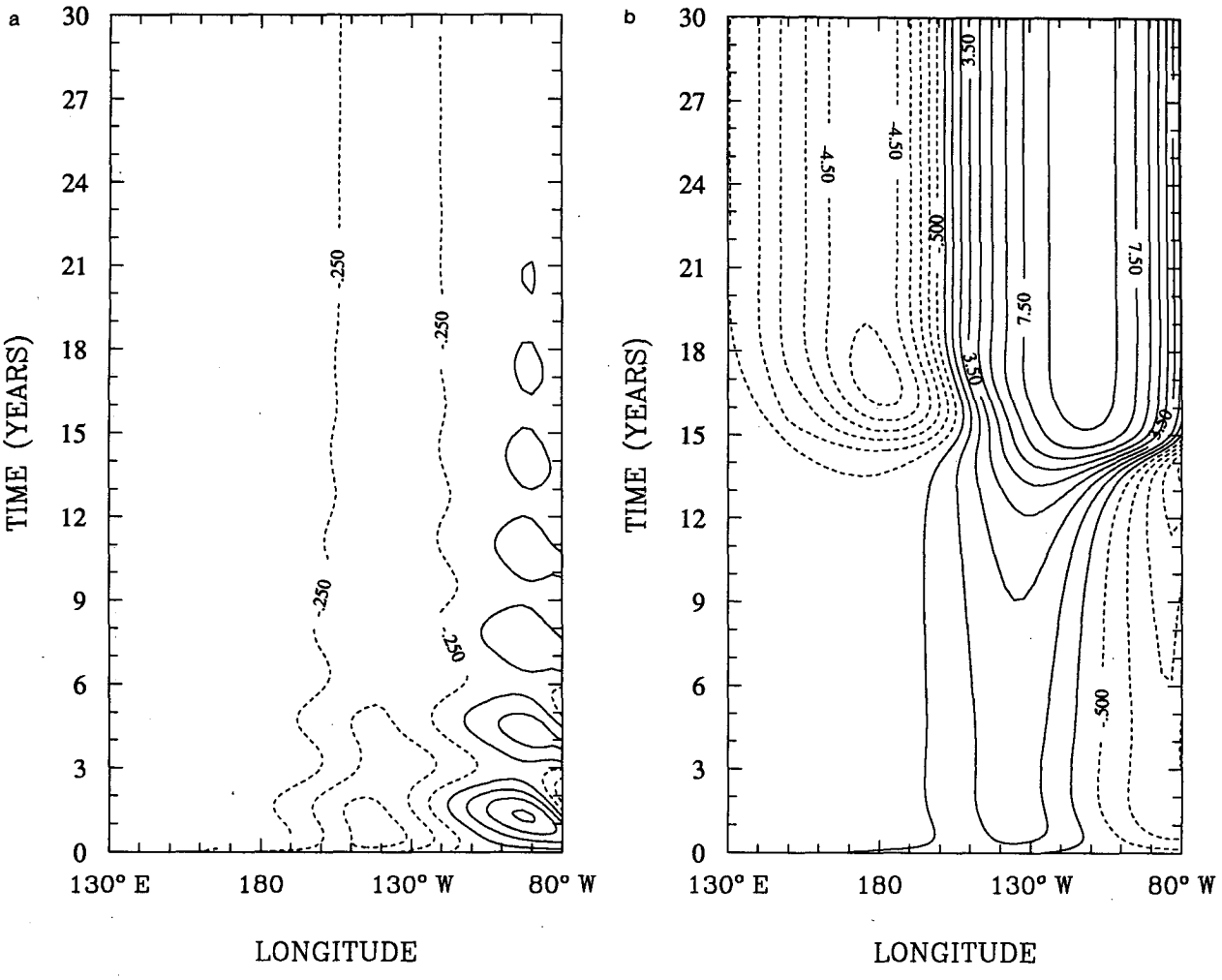

FIG. 12. SST anomaly as in Fig. 6 (intermediate surface-layer feedback) but for $\mu = 0.675$. In this case, only two stationary points exist: (a) cold state and (b) extreme warm stationary state.

Figure 13 shows the situation for a very slightly larger coupling, $\mu = 0.705$. The warm state branch has changed little, although the system tends to reach it much faster when starting from the same initial state close to the climatology, consistent with the above interpretation. The cold-state branch has gone unstable in a Hopf bifurcation, however, yielding a limit cycle with a 3-year period. The oscillation is westward propagating and confined to the east of the date line. It is very closely related in form and mechanism to the westward-propagating mode, which is the second most unstable mode for the system linearized about climatology. For these intermediate parameter values, there is a substantial standing component to the oscillation.

Again increasing coupling, a small range of complex behavior is encountered (Fig. 14a). A tertiary bifurcation has introduced an additional period into the oscillation about the cold state and possibly there has been a transition to aperiodic behavior—there are no exact repeats within the 30 years shown, although the flow is very close to a that of a torus with two periodicities. This regime is not very extensive, however, and so it is not felt that great emphasis can be placed on it. A tiny increase in μ (Fig. 14b) leads to a situation where the oscillation is unstable and leads to the extreme warm stationary state. Indeed, for a large number of runs with $\mu > 0.72$ near this intermediate value or larger values of δ_s, this extreme warm state is the only attractor that has been found.

5. Summary and discussion

The linear and nonlinear behavior of SST modes in the fast-wave limit are investigated in a simple ocean model coupled with a simple Gill model atmosphere. In the fast-wave limit in a finite basin, equatorial wave dynamics enters the boundary conditions, but the time scales of wave dynamics are assumed fast compared to the evolution of SST due to coupled processes. At any given time in the model, ocean dynamics is always in

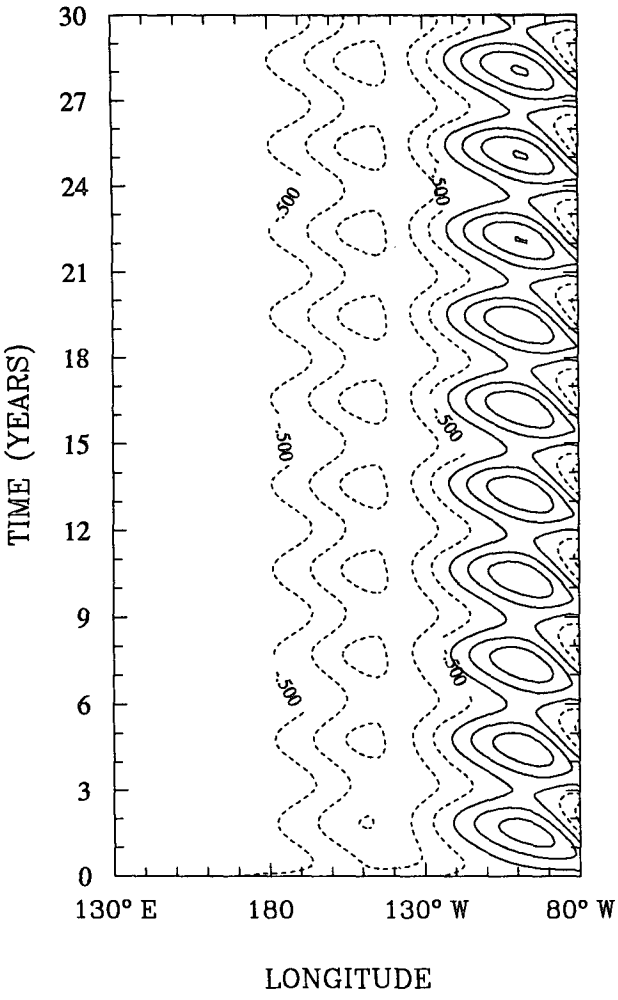

FIG. 13. SST anomaly as in Fig. 12a but for $\mu = 0.705$. In this case the cold state has bifurcated to a limit cycle.

adjustment with the wind stress and any time dependence enters due to the coupled interactions in the SST equation. This model thus offers a converse approximation to what may be termed the fast-SST limit used by Cane et al. (1990), Münnich et al. (1991), and Schopf and Suarez (1990) in which SST is assumed to be in instantaneous adjustment, and time dependence is due entirely to the time scales of ocean wave dynamics. Jin and Neelin (1993a,b) discuss the relation between these models, fast-wave limit models, and the oscillations found in intermediate coupled models (Zebiak and Cane 1987; Battisti 1988), and to the simple delay oscillator equation discussed by Shopf and Suarez (1988) and Battisti and Hirst (1989), showing how they may all be understood as approximations to the same continuous surface of eigenvalues in parameter space. Our emphasis here is on the use of an SST equation that is close to that used in intermediate models and on the implications of this for nonlinear interactions.

Two main feedback processes have been considered here: one associated with thermocline perturbations and the other with upwelling perturbations due to surface-layer currents. Both of them contribute to the growth of the SST mode but tend to give different directions of propagation: eastward when the thermocline feedback dominates and westward when the surface-layer feedback dominates. For a fair range of coupling above the respective Hopf bifurcations in these propagating cases, the resulting interannual oscillations bear considerable resemblance to ENSO-like oscillations both in some coupled models and in a number of observed aspects. Without claiming that the fast-wave limit provides a perfect match for such oscillations in other models, it does serve as a simple analog for some of the processes involved. Perhaps as importantly, the complexity of the spatial and temporal evolution of these oscillations, in which wave time scales are explicitly excluded, serves as a caution against overinterpretation of coupled models based on visual inspection alone. Much of the parameter dependence of these oscillations may be qualitatively explained from the periodic-basin case, while the finite basin and spatially varying basic state introduce east-basin trapping.

An important feature of the finite-basin case, not found in the periodic basin, is the existence of a stationary, purely growing mode over significant regions of parameter space. It can arise either from a balance of westward and eastward propagation tendencies or from the effects of finite-basin boundary conditions on the thermocline feedback and atmospheric response. The atmospheric damping length, for instance, influences the transition between the stationary growth regime and an eastward-propagating regime, since when it is small the response tends to be more localized and less influenced by basin boundary conditions. Jin and Neelin (1993a,b) discuss how this stationary mode can be mixed with wave time-scale effects to produce an oscillatory mode when sufficiently far from the fast-wave limit and for coupling that is not too strong. The bifurcations associated with the fast-wave limit stationary mode discussed here may thus be expected to apply both close to the fast-wave limit and for relatively strong coupling versus damping balances in a system that includes wave dynamics.

The stationary mode gives rise to warm and cold stationary states through a transcritical bifurcation and a number of limit points. An even simpler analog model demonstrates qualitatively how the stationary branches yield one, two, or three stable stationary points in different parameter ranges. In addition to stationary points directly related to small-amplitude equilibrated versions of the unstable stationary mode near the climatological stationary point, an extreme warm stationary state can exist. This state is associated with the upwelling–downwelling nonlinearity and corresponds to a near-total shutdown of the climatological upwelling by reversal of the trade winds. This state

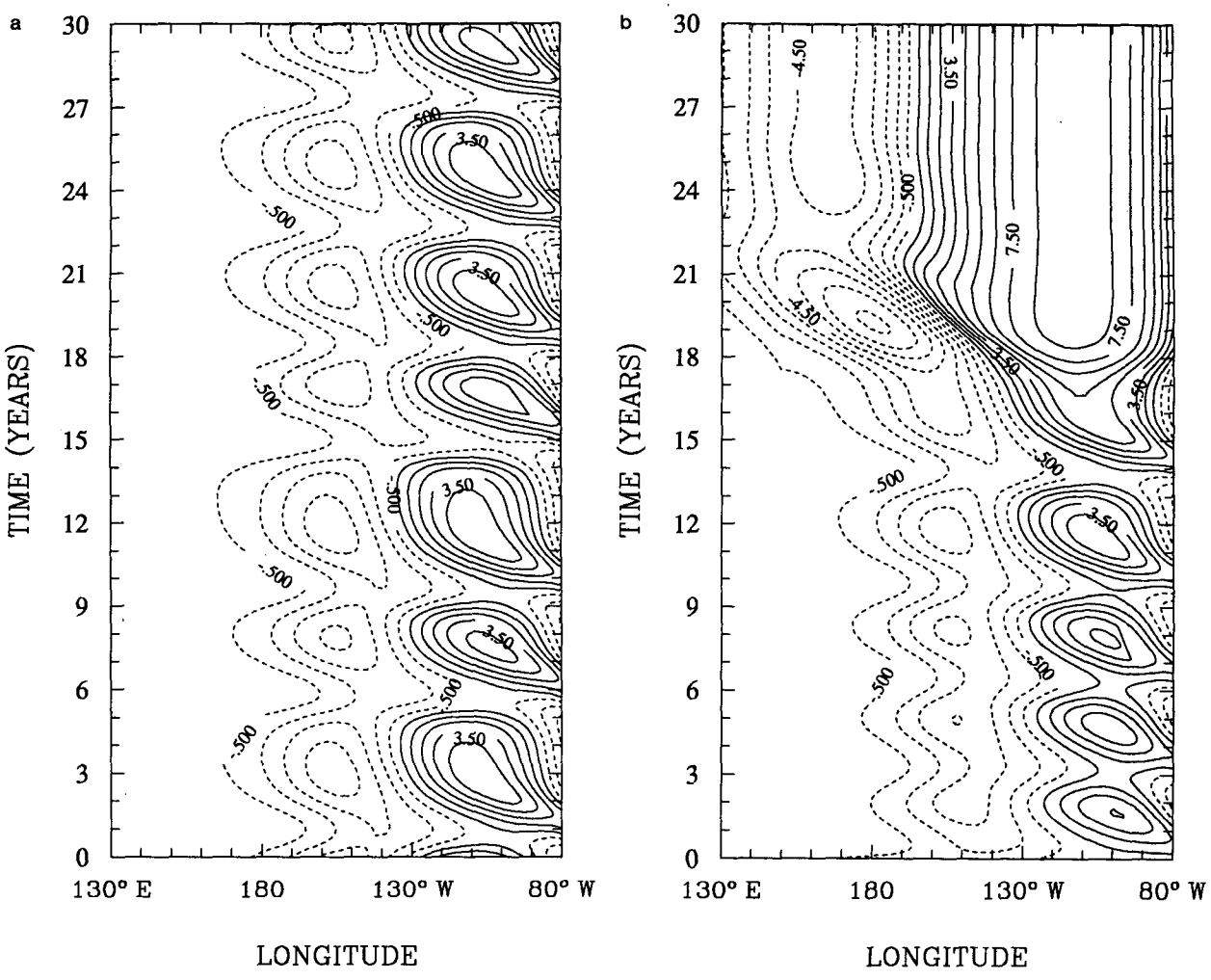

FIG. 14. SST anomaly as in Fig. 12a but (a) for $\mu = 0.7125$ and (b) for $\mu = 0.713$.

exists and is stable over a very large range of parameters at sufficiently high coupling. It is worth questioning how realistic this state is, given that the climatological stationary state has been constructed. At the very least, it gives an indication of what can happen in other models that specify climatology or use flux correction. In fact, it likely provides a good understanding of how a similar state arises in the hybrid coupled GCM of Neelin (1990b) and may give insight into the behavior of the Cane and Zebiak model in some regimes. It should be noted, however, that the total wind stress amplitude need not be very high in this state since the anomalies simply tend to cancel the climatological easterlies. The implication is that a weak westerly state can be a consistent solution over a wide range of coupling. This suggests that perhaps it is the constructed climatological state that is more open to question at both high and low coupling when strong nonlinearity is considered. It seems likely that the bifurcation diagram for the total coupled system, beginning from an uncoupled, radiative equilibrium state rather than a constructed climatology, could have features related to those found here.

Another robust feature of the system is the presence of relaxation oscillations for moderately high coupling. As coupling is increased for oscillatory cases, whether eastward or westward propagating, the period of the oscillation increases as one of the phases encounters strong limiting nonlinearity. When the oscillation is dominated by the upwelling feedback (i.e., westward propagating), the warm phase tends to have significant decreases in upwelling, thus reducing the rate of change during the warm phase. As the amplitude of the cycle becomes larger, this slow warm phase lengthens and comes to resemble the extreme warm stationary state. Presumably this extended phase of the relaxation oscillation is passing very close to the unstable warm stationary state that must lie in between. At still higher coupling, the oscillation disappears entirely, and the flow enters the extreme warm stationary state.

In flow regimes where the oscillation is dominated by the thermocline feedback, the limiting nonlinearity

tends to be encountered first in the cold phase in the eastern Pacific, where the climatological thermocline is already shallow. During the cold phase, further shallowing produces a decrease in the sensitivity of subsurface temperature to thermocline changes and thus a decreased rate of change. At high coupling, this results in a relaxation oscillation with a lengthened cold phase. It again appears that the relaxation oscillation is associated with interaction of the oscillation with a stationary state, since the transition to a cold stationary state with increased coupling occurs in a similar manner to the warm case, although at higher coupling. It is noteworthy that these relaxation oscillations occur over a very wide range of parameters (e.g., for surface-layer feedbacks from very strong to zero) when oscillatory regimes reach high amplitudes.

The relation between propagating and stationary modes in neighboring regions of parameter space can be complex. Two types of transition can mark the boundary between oscillatory (in this case propagating) and stationary regimes: 1) a complex conjugate pair of eigenvalues can merge to a double zero and become two pure real eigenvalues, one growing and one decaying; 2) a complex conjugate pair can become stable just as a stationary mode becomes unstable (pure imaginary pair and a simple zero eigenvalue). These are codimension-2 bifurcations [following the convention of Guckenheimer and Holmes (1983)] and the parameter values for which they can occur form surfaces of dimension $n - 2$ for a parameter space of dimension n. Jin and Neelin (1993a,b) emphasize the importance to the coupled system of the first type, in which an oscillatory mode is transformed continuously into a stationary mode. The growing stationary and oscillatory modes on either side of the bifurcation necessarily bear some resemblance to one another and it can be useful to think of them as being in some sense the same mode in that they are continuously connected. An example of this is the stationary mode to eastward-propagating mode transition. Here we further encounter an example of the second type, in which a stationary mode "overtakes" an oscillatory mode as one of the parameters (e.g., strength of surface-layer feedback) is changed and becomes the mode that first goes unstable as the other parameter (e.g., coupling strength) is changed to keep the system near the bifurcation.

The two modes have only slightly different growth rates over an appreciable range of parameters (for intermediate strengths of surface-layer feedback). The mode interaction between these can produce quite a complicated bifurcation diagram in this range, which we have explored only partially, on the side where the stationary mode produces the first bifurcation. In addition to the subtleties of the limit point for the weak warm stationary branch mentioned above, the cold branch becomes unstable to a mode essentially identical to the propagating secondmost unstable mode near the climatology. This limit cycle bifurcates to a complicated flow that appears to involve period doubling and may be mildly chaotic, but this regime is so restricted that it is unlikely to be of great physical consequence. At very high coupling, extreme warm and/or cold stationary states appear to be the only attractors.

The complexity of the flow regimes that can develop even in this simplified model is an indication of the richness of the coupled system. While not all the regimes examined here are close to the observed system, some bear suggestive similarities both to observations and to more complex coupled models, and experience suggests that mapping out a substantial range of possible behaviors can yield valuable insight into the relationships between these. It was argued in JN that the fast-wave limit is a useful point of departure for understanding the linear modes of the fully coupled system since the modes in the most realistic regime are closely related and the fast-wave limit can provide analytical insight into spatial structures and mechanisms of instability. The results presented here suggest that the fast-wave limit can also provide a useful prototype for some of the nonlinear interactions that may occur in intermediate models and GCMs and, by extension, in the observed system.

Acknowledgments. This work was supported in part by NSF Grants ATM-9215090 (JDN and FFJ) and ATM-9158294 (JDN), NOAA Grant NA26GP0114-01 (ZH), and ONR Grant N00014-89-1845 (ZH). Our appreciation is expressed to M. Ghil for patient encouragement and support. We thank M. Cane for a friendly and stimulating correspondence (Cane 1992; Neelin et al. 1992b), which provided an earlier forum for expressing some of the arguments presented here, and G. Philander and I. Held for discussions of earlier versions of this work. We thank H. Dijkstra for a careful reading of the manuscript and for ongoing work on the bifurcation diagram.

REFERENCES

Anderson, D. L. T., and J. P. McCreary, 1985: Slowly propagating disturbances in a coupled ocean-atmosphere model. *J. Atmos. Sci.*, **42**, 615–628.

Barnett, T. P., 1991: The interaction of multiple time scales in the tropical climate system. *J. Climate*, **4**, 269–285.

Battisti, D. S., 1988: The dynamics and thermodynamics of a warm event in a coupled atmosphere–ocean model. *J. Atmos. Sci.*, **45**, 2889–2919.

——, 1989: On the role of off-equatorial oceanic Rossby waves during ENSO. *J. Phys. Oceanogr.*, **19**, 551–559.

——, and Hirst, A. C., 1989: Interannual variability in the tropical atmosphere/ocean system: Influence of the basic state and ocean geometry. *J. Atmos. Sci.*, **45**, 1687–1712.

Bjerknes, J., 1969: Atmospheric teleconnections from the equatorial Pacific. *Mon. Wea. Rev.*, **97**, 163–172.

Cane, M. A., 1979: The response of an equatorial ocean to simple wind stress patterns. I: Model formulation and analytic results. *J. Mar. Res.*, **A 37**, 233–252.

——, 1992: A note on the fast-wave limit and interannual oscillations. *J. Atmos. Sci.*, **49**, 1947–1949.

——, and E. S. Sarachik, 1981: The response of a linear baroclinic equatorial ocean to periodic forcing. *J. Mar. Res.*, **39**, 651–693.

——, and S. E. Zebiak, 1985: A theory for El Niño and the southern Oscillation. *Science,* **228,** 1084–1087.

——, M. Münnich, and S. E. Zebiak, 1990: A study of self-excited oscillations of the tropical ocean–atmosphere system. Part I: Linear analysis. *J. Atmos. Sci.,* **47,** 1562–1577.

Deser, C., and J. M. Wallace, 1987: El Niño events and their relation to the Southern Oscillation: 1925–1986. *J. Geophys. Res.,* **92c,** 14 189–14 196.

Ghil, M., and R. Vautard, 1991: Interdecadal oscillations and the warming trend in global temperature time series. *Nature,* **350,** 324–327.

Gill, A. E., 1980: Some simple solutions for heat induced tropical circulation. *Quart. J. Roy. Meteor. Soc.,* **106,** 447–462.

Golubitsky, M., I. Stewart, and D. G. Schaeffer, 1988: *Singularities and Groups in Bifurcation Theory,* Vol II. Springer-Verlag, 533 pp.

Graham, N. E., and W. B. White, 1988: The El Niño cycle: Pacific ocean–atmosphere system. *Science,* **240,** 1293–1302.

——, J. Michaelsen, and T. P. Barnett, 1987: An investigation of the El Niño–Southern Oscillation cycle with statistical models. 1: Predictor field characteristics. *J. Geophys. Res.,* **92,** 14 251–14 270.

Guckenheimer, J., and P. Holmes, 1983: *Nonlinear Oscillations, Dynamical Systems and Bifurcations of Vector Fields.* Springer-Verlag, 459 pp.

Hirst, A. C., 1986: Unstable and damping equatorial modes in simple coupled ocean–atmosphere models. *J. Atmos. Sci.,* **43,** 606–632.

——, 1988: Slow instabilities in tropical ocean-basin–global-atmosphere models. *J. Atmos. Sci.,* **45,** 830–852.

Jin, F.-F., and J. D. Neelin, 1993a: Modes of interannual tropical ocean–atmosphere interaction—A unified view. Part I: Numerical results. *J. Atmos. Sci.,* **50** (21) in press.

——, and ——, 1993b: Modes of interannual tropical ocean–atmosphere interaction—A unified view. Part III: Analytical results in fully coupled cases. *J. Atmos. Sci.,* **50** (21) in press.

Keller, H. B., 1977: Numerical solution of bifurcation and nonlinear eigenvalue problems. *Applications of Bifurcation Theory,* P. H. Rabinowitz, Ed., Academic Press, 389 pp.

Latif, M., and A. Villwock, 1990: Interannual variability in the tropical Pacific as simulated in a coupled ocean–atmosphere models. *J. Mar. System,* **1,** 51–60.

——, A. Sterl, E. Maier-Reimer, and M. M. Junge, 1993: Climate variability in a coupled GCM. Part I: the tropical Pacific. *J. Climate,* **6,** 5–21.

Lau, N. C., S. G. H. Philander, and M. J. Nath, 1992: Simulation of El Niño–Southern oscillation phenomena with a low-resolution coupled general circulation model of the global ocean and atmosphere. *J. Climate,* **5,** 284–307.

Lindzen, R. S., and S. Nigam, 1987: On the role of sea surface temperature gradients in forcing low level winds and convergence in the tropics. *J. Atmos. Sci.,* **44,** 2440–2458.

Meehl, G. A. 1990: Development of global coupled ocean–atmosphere general circulation models. *Climate Dyn.,* **5,** 19–33.

Münnich, M., M. A. Cane, and S. E. Zebiak, 1991: A study of self-excited oscillations in a tropical ocean–atmosphere system. Part II: Nonlinear cases. *J. Atmos. Sci.,* **48,** 1238–1248.

Nagai, T., T. Tokioka, M. Endoh, and Y. Kitamura, 1992: El Niño–Southern oscillation simulated in an MRI atmosphere ocean coupled GCM. *J. Climate,* **5,** 1202–1233.

Neelin, J. D., 1988: A simple model for surface stress and low-level flow in the tropical atmosphere driven by prescribed heating. *Quart. J. Roy. Meteor. Soc.,* **114,** 747–770.

——, 1989a: Interannual oscillations in an ocean general circulation model coupled to a simple atmosphere model. *Phil. Trans. Roy. Soc. London,* **A329,** 189–205.

——, 1989b: A note on the interpretation of the Gill model. *J. Atmos. Sci.,* **46,** 2466–2468.

——, 1990a: A hybrid coupled general circulation model for El Niño studies. *J. Atmos. Sci.,* **47,** 674–693.

——, 1990b: Bifurcations and El Niño in a hybrid coupled GCM. *Proc. 14th Climate Diagnostics Workshop,* San Diego, CA, Climate Analysis Center, National Oceanic and Atmospheric Administration, 22–27.

——, 1991: The slow sea surface temperature mode and the fast-wave limit: Analytic theory for tropical interannual oscillations and experiments in a hybrid coupled model. *J. Atmos. Sci.,* **48,** 584–606.

——, and I. M. Held, 1987: Modeling tropical convergence based on the moist static energy budget. *Mon. Wea. Rev.,* **115,** 3–12.

——, and F.-F. Jin, 1993: Modes of interannual tropical ocean–atmosphere interaction—A unified view. Part II: Analytical results in the weak coupling limit. *J. Atmos. Sci.,* **50** (21) in press.

——, M. Latif, M. A. F. Allaart, M. A. Cane, U. Cubasch, W. L. Gates, P. R. Gent, M. Ghil, C. Gordon, N. C. Lau, C. R. Mechoso, G. A. Meehl, J. M. Oberhuber, S. G. H. Philander, P. S. Schopf, K. R. Sperber, A. Sterl, T. Tokioka, J. Tribbia, and S. E. Zebiak, 1992a: Tropical air–sea interaction in general circulation models. *Climate Dyn.,* **7,** 73–104.

——, Z. Hao, and F.-F. Jin, 1992b: Reply. *J. Atmos. Sci.,* **49,** 1950–1953.

Philander, S. G. H., and Y. Chao, 1991: On the contrast between the seasonal cycle of the equatorial Atlantic and Pacific oceans. *J. Phys. Oceanogr.,* **21,** 1399–1406.

——, R. C. Pacanowski, N. C. Lau, and M. J. Nath, 1992: A simulation of the Southern Oscillation with a global atmospheric GCM coupled to a high-resolution, tropical Pacific ocean GCM. *J. Climate,* **5,** 308–329.

——, T. Yamagata, and R. C. Pacanowski, 1984: Unstable air–sea interactions in the tropics. *J. Atmos. Sci.,* **41,** 604–613.

Rasmusson, E. M., and T. H. Carpenter, 1982: Variations in tropical sea surface temperature and surface wind fields associated with the Southern Oscillation–El Niño. *Mon. Wea. Rev.,* **110,** 354–384.

——, X. Wang, and C. F. Ropelewski, 1990: The biennial component of ENSO variability. *J. Mar. Syst.,* **1,** 71–96.

Schopf, P. S., and M. J. Suarez, 1988: Vacillations in a coupled ocean–atmosphere model. *J. Atmos. Sci.,* **45,** 549–566.

——, and ——, 1990: Ocean wave dynamics and the time scale of ENSO. *J. Phys. Oceanogr.,* **20,** 629–645.

Suarez, M. J., and P. S. Schopf, 1988: A delayed action oscillator for ENSO. *J. Atmos. Sci.,* **45,** 3283–3287.

Wakata, Y., and E. S. Sarachik, 1991: On the role of equatorial ocean modes in the ENSO cycle. *J. Phys. Oceanogr.,* **21,** 434–443.

Yamagata, T., and Y. Masumoto, 1989: A simple ocean–atmosphere coupled model for the origin of a warm El Niño Southern Oscillation event. *Phil. Trans. Roy. Soc. London,* **A329,** 225–236.

Yang, J., and J. J. O'Brien, 1993: A coupled atmosphere–ocean model in the tropics with different thermocline profiles. *J. Climate,* **6,** 1027–1040.

Zebiak, S. E., and M. A. Cane, 1987: A model El Nino–Southern Oscillation. *Mon. Wea. Rev.,* **115,** 2262–2278.